

# The Formation of Supermassive Black Holes from Population III.1 Seeds. I. Cosmic Formation Histories and Clustering Properties

Nilanjan Banik<sup>1,2,3,4</sup>, Jonathan C. Tan<sup>5,6</sup>, Pierluigi Monaco<sup>7,8,9</sup>

<sup>1</sup>*Dept. of Physics, University of Florida, Gainesville, FL 32611, USA,*

<sup>2</sup>*Fermi National Accelerator Laboratory, Batavia, IL 60510-0500, USA*

<sup>3</sup>*GRAPPA Institute, Institute for Theoretical Physics Amsterdam*

*and Delta Institute for Theoretical Physics, University of Amsterdam, Science Park 904, 1098 XH Amsterdam, The Netherlands,*

<sup>4</sup>*Lorentz Institute, Leiden University, Niels Bohrweg 2, Leiden, 2333 CA, The Netherlands,*

<sup>5</sup>*Dept. of Space, Earth & Environment, Chalmers University of Technology, SE-412 93 Gothenburg, Sweden*

<sup>6</sup>*Dept. of Astronomy, University of Virginia, 530 McCormick Road, Charlottesville, VA 22904-4325, USA*

<sup>7</sup>*Università di Trieste, Dipartimento di Fisica, Sezione di Astronomia, via Tiepolo 11, 34143 Trieste, Italy,*

<sup>8</sup>*INAF-Osservatorio Astronomico di Trieste, via Tiepolo 11, 34143 Trieste, Italy,*

<sup>9</sup>*INFN, via Valerio 2, I-34127 Trieste, Italy*

3 December 2018

## ABSTRACT

We calculate cosmic distributions in space and time of the formation sites of the first, “Pop III.1” stars, exploring a model in which these are the progenitors of all supermassive black holes (SMBHs), seen in the centers of most large galaxies. Pop III.1 stars are defined to form from primordial composition gas in dark matter minihalos with  $\sim 10^6 M_\odot$  that are isolated from neighboring astrophysical sources by a given isolation distance,  $d_{\text{iso}}$ . We assume Pop III.1 sources are seeds of SMBHs, based on protostellar support by dark matter annihilation heating that allows them to accrete a large fraction of their minihalo gas, i.e.,  $\sim 10^5 M_\odot$ . Exploring  $d_{\text{iso}}$  from 10–100 kpc (proper distances), we predict the redshift evolution of Pop III.1 source and SMBH remnant number densities. The local,  $z = 0$  density of SMBHs constrains  $d_{\text{iso}} \lesssim 100$  kpc (i.e., 3 Mpc comoving distance at  $z \simeq 30$ ). In our simulated ( $\sim 60$  Mpc)<sup>3</sup> comoving volume, Pop III.1 stars start forming just after  $z = 40$ . Their formation is largely complete by  $z \simeq 25$  to 20 for  $d_{\text{iso}} = 100$  to 50 kpc. We follow source evolution to  $z = 10$ , by which point most SMBHs reside in halos with  $\gtrsim 10^8 M_\odot$ . Over this period, there is relatively limited merging of SMBHs for these values of  $d_{\text{iso}}$ . We also predict SMBH clustering properties at  $z = 10$ : feedback suppression of neighboring sources leads to relatively flat angular correlation functions.

## 1 INTRODUCTION: THE ORIGIN OF SUPERMASSIVE BLACK HOLES

Baryonic collapse appears to lead to two distinct populations of objects: (1) stars (and associated planets); (2) supermassive black holes (SMBHs), i.e., with masses  $\gtrsim 10^5 M_\odot$ . Accretion to SMBHs powers active galactic nuclei (AGN) and this feedback is thought to play a crucial role in the evolution of galaxies, e.g., maintaining high gas temperatures and thus impeding cooling flows and continued star formation in galaxy clusters.

In spite of their importance, as discussed below, there is no settled theory for the formation of SMBHs. Simulations and models of galaxy formation and evolution typically make ad hoc assumptions about the creation of these objects. For example, in the Illustris simulation (Vogelsberger et al. 2014), following methods developed by Sijacki et al. (2007) and Di Matteo et al. (2008), SMBHs are simply created with initial masses of  $1.4 \times 10^5 M_\odot$  in every dark matter

halo that crosses a threshold mass of  $7 \times 10^{10} M_\odot$ . Barber et al. (2016) follow a similar method in the EAGLE simulation. In the semi-analytic models of Somerville et al. (2008), dark matter halos with  $> 10^{10} M_\odot$  are seeded with black holes with a variety of initial masses explored from 100 to  $10^4 M_\odot$ . Shirakata et al. (2016) have also explored the effects of the choice of seed black hole mass in their semi-analytic models of galaxy formation and evolution. Black holes are created in every “galaxy,” i.e., every halo that is able to undergo atomic cooling. Their models with massive ( $10^5 M_\odot$ ) seed black holes lead to a black hole mass versus bulge mass relation that is too high, especially compared to that observed for lower mass ( $\sim 10^9 M_\odot$ ) bulges of dwarf galaxies (Graham & Scott 2015). Thus Shirakata et al. prefer models with lower seed masses, e.g., randomly drawn from  $10^3$  to  $10^5 M_\odot$ , but other solutions may also be possible, such as reducing the SMBH occurrence fraction in lower-mass galaxies. For example, Fontanot et al. (2015) present a model that ex-

plains the break in the black hole versus bulge relation of Scott & Graham (2015) as an indirect effect of stellar feedback in the spheroidal component of galaxies, starting with  $10^5 M_\odot$  SMBH seeds.

The overall goal of this paper is to explore a relatively new physical mechanism for SMBH formation as the outcome of the evolution of Population III.1 stars, which are primordial composition (i.e., Pop III) stars that are the first objects to form in their local regions of the universe, thus being undisturbed by the feedback from other astrophysical sources (McKee & Tan 2008). In particular, since the formation locations and times of Pop III.1 stars can be predicted by standard models of cosmological structure formation based on the growth of halos of cold dark matter (CDM), we aim to predict the formation histories and clustering properties of SMBHs forming via this mechanism. This will allow eventual testing of the model against future observations of high-redshift SMBHs, as well as the properties of more local SMBH populations.

### 1.1 Constraints from the Properties of Local and Distant SMBHs

From studies of the local universe, SMBHs have masses  $\gtrsim 10^5 M_\odot$  and are found in the centers of most large galaxies that have spheroidal stellar components (e.g., Kormendy & Ho 2013; den Brok et al. 2015; see reviews by Graham 2016 and Reines & Comastri 2016). The lowest mass SMBH that has been reported is the  $\sim 50,000 M_\odot$  example in the nucleus of RGG 118 (Baldassare et al. 2015). However, a number of nearby dwarf galaxies as well as spiral galaxies with small bulges, e.g., M33, have estimated upper limits on the presence of a SMBH that are close to  $\sim 10^4 M_\odot$ . No nuclear SMBH has yet been detected directly, e.g., via its optical or X-ray emission, in a galaxy with a stellar mass  $< 10^8 M_\odot$ . There are some claimed indirect detections of SMBHs in ultracompact dwarf galaxies (UCDs) (Seth et al. 2014; Ahn et al. 2017) from dynamical modeling, but these UCDs are expected to be the tidally stripped remnants of more massive galaxies, originally with  $\gtrsim 10^9 M_\odot$  stellar masses.

There have been some claims for the existence of intermediate-mass black holes (IMBHs), i.e., with masses in the range  $\sim 100$  to  $\sim 10^5 M_\odot$  that bridge the gap between stellar mass remnants and SMBHs. The presence of IMBHs within the centers of globular clusters (GCs) has been reported based on stellar kinematics. However, in the recent analysis of Baumgardt (2017) in which grids of  $N$ -body simulations with and without IMBHs are compared to 50 observed Galactic GCs, only one system,  $\omega$  Cen (NGC 5139),

is shown to have a clear kinematic signature that may indicate the presence of an IMBH (of  $\sim 40,000 M_\odot$ ). However, as discussed by Baumgardt (2017), this is not a unique interpretation, with other possibilities being the presence of radially anisotropic velocity dispersion profiles within the cluster (Zocchi, Gieles & Hénault-Brunet 2016). In another individual case, Kızıltan, Baumgardt & Loeb (2017) have reported a  $2200_{-800}^{+1500} M_\odot$  black hole in the center of the globular cluster 47 Tucanae based on the observed kinematics of pulsars. However, more generally there is no evidence yet for the expected accretion signatures of IMBHs in globular clusters (e.g., Kirsten & Vlemmings 2012; Wrobel, Miller-Jones & Middleton 2016). For example, Wrobel et al. (2016) re-

port only upper limits based on deep cm radio continuum observations of 206 GCs in M81, although their  $3\sigma$  upper limit on the mean black hole mass of  $\sim 50,000 M_\odot$  in the most massive GCs is not that restrictive and is dependent on the modeling of accretion and radio emission of the putative IMBHs.

Ultra-luminous X-ray sources (ULXs) away from the nuclei of their host galaxies and with X-ray luminosities  $L_X > 10^{39} \text{ erg s}^{-1}$  (i.e., greater than the Eddington luminosity of a  $10 M_\odot$  black hole) have been detected and proposed as being evidence for IMBHs. For example, the source ESO 243-49 HLX1 with  $L_X \sim 10^{42} \text{ erg s}^{-1}$  and an estimated black hole mass of  $M_{\text{BH}} \sim 10^4\text{--}10^5 M_\odot$  in a cluster with a stellar mass of  $M_* \sim 10^5\text{--}10^6 M_\odot$  has been claimed by Farrell et al. (2014). The source M82 X1 with  $L_X \sim 5 \times 10^{40} \text{ erg s}^{-1}$  from a  $400 M_\odot$  black hole has been discussed by Feng et al. (2010) and Pasham et al. (2014). However, NGC 5643 ULX1 with  $L_X > 10^{40} \text{ erg s}^{-1}$  has been modeled as a  $30 M_\odot$  black hole that is undergoing super-Eddington accretion and/or beaming its emission preferentially in our direction (Pintore et al. 2016). Overall, there are relatively few clear examples of ULXs that present unambiguous evidence for IMBHs, with the majority thought to be explainable as stellar mass black holes in X-ray binaries that are undergoing active accretion from massive stellar companions (Zampieri & Roberts 2009; Feng & Soria 2011).

Some SMBHs appear to have reached masses  $\sim 10^9 M_\odot$  by  $z \simeq 7$  ( $t \simeq 800$  Myr after the Big Bang) (e.g., Mortlock et al. 2011; however, see the factor of  $\sim 5$  lower revised mass estimates of Graham et al. 2011; Shankar et al. 2016). However, such objects are rare: an estimate of the  $z \sim 6$  quasar luminosity function finds a number density of observed sources of  $\sim 10^{-8} \text{ Mpc}^{-3}$  (Willott et al. 2010; see also Treister et al. 2013).

There seems to be a relative dearth of actively accreting lower-mass SMBHs at  $z \sim 6$ , based on the flat faint-end slope of the X-ray luminosity function (XLF) derived from a stacking analysis of the Chandra Deep Field South (Vito et al. 2016) and the lack of X-ray AGN in  $z \gtrsim 6$  Lyman break galaxies (Cowie, Barger & Hasinger 2012; Fiore et al. 2012; Treister et al. 2013).

In summary, there appears to be a characteristic minimum mass of SMBHs of  $\sim 10^5 M_\odot$ , with most low-mass galaxies lacking the presence of any such object, and relatively limited evidence for IMBHs. Such properties of the SMBH population are a constraint on theories of their formation. In particular, they may indicate that the initial seed mass is relatively massive, i.e.,  $\sim 10^5 M_\odot$ , and that not all galaxies are seeded with SMBHs.

### 1.2 Theoretical Models of SMBH Formation

SMBH formation scenarios have been discussed for many years (e.g., Rees 1978). One popular model is “direct collapse” of massive, primordial composition gas clouds, which is thought to require strong UV (Lyman-Werner) radiation fields to dissociate  $\text{H}_2$  molecules and thus prevent cooling to  $\sim 200$  K and fragmentation to  $\sim 100 M_\odot$  mass scales, but also requires dark matter halo virial temperatures  $\gtrsim 8,000$  K (i.e., masses  $\gtrsim 10^8 M_\odot$ ) (e.g., Haehnelt & Rees 1993; Bromm & Loeb 2003; Begelman et al. 2006; Dijkstra et al. 2006; Ferrara & Loeb 2013; Dijkstra et al. 2014; Chon et al. 2016).

The high accretion rates that occur in the centers of these halos may allow the formation of supermassive stars, which then collapse to form SMBHs (e.g., Inayoshi et al. 2013; Umeda et al. 2016). The study of Chon et al. (2016) examined a  $(20h^{-1} \text{Mpc})^3$  volume to search for dark matter halos meeting these criteria, finding about 50 candidates that form at  $z \sim 10$  to 20. However, only two of these were seen to undergo collapse, with the others mostly disrupted by mergers, tidal disruptions and/or ram pressure stripping with neighboring halos. While the number density of successful direct collapse events in their model, i.e.,  $\sim 10^{-4} \text{Mpc}^{-3}$ , is greater than the observed number density of high- $z$  SMBHs, it is much smaller than the total comoving number density of SMBHs observed at  $z = 0$  ( $\sim 10^{-3}$ – $10^{-2} \text{Mpc}^{-3}$ ; see §3.1), so it may be difficult for this mechanism to form all SMBHs. One possibility that could boost the number density of direct collapse events, discussed by Chon et al., is that their adopted critical UV flux to prevent  $\text{H}_2$  formation is too conservative. However, as also discussed by Chon et al., the modeling of direct collapse halos to make accurate predictions of event rates is very challenging, since it requires making a number of uncertain assumptions about the star formation in the early universe that sets the UV feedback environments necessary for this model.

An alternative model that may create the conditions for direct collapse has been proposed by Mayer et al. (2010; 2015) involving rapid infall of gas driven by mergers of gas-rich massive galaxies occurring at  $z \sim 4$ –10. This scenario does not require primordial composition gas, with fragmentation and star formation of the gas suppressed by gravity-driven turbulence and torques. Up to  $\sim 10^9 M_\odot$  of gas is proposed to be able to accumulate on sub-parsec scales, leading to ultra-massive black hole seeds of  $\sim 10^8 M_\odot$ . However, as discussed by Mayer et al. (2015), caveats of this model include that the supporting simulation results are based on binary collisions of gas-rich galaxies rather than being self-consistently extracted from cosmological simulations. Estimates of the frequency of black hole formation via this scenario are quite uncertain, although potentially high enough to explain the observed high  $z$  quasar population.

Yet another model involves high ( $\gtrsim 200 \text{km s}^{-1}$ ) velocity collisions of protogalaxies that create hot, dense gas that leads to collisional dissociation of  $\text{H}_2$  molecules (Inayoshi & Omukai 2012; Inayoshi et al. 2015). However, the comoving number density of black holes formed by such a mechanism is estimated to be only  $\sim 10^{-9} \text{Mpc}^{-3}$  by  $z \sim 10$ , which, while it may be enough to help explain observed high  $z$  quasars, is too small to explain all SMBHs.

Another scenario for IMBH or SMBH formation involves a very massive stellar seed forming in the center of a dense stellar cluster by a process of runaway mergers (Gürkan et al. 2004; Portegies Zwart et al. 2004; Freitag et al. 2006). However, the required central stellar densities are extremely high (never yet observed in any young cluster) and also stellar wind mass loss may make growth of the central very massive star quite inefficient (Vink 2008), unless the metallicities are very low (Devecchi et al. 2012). Again, predictions of such models for the cosmic formation rates of SMBHs are limited since it is difficult to predict when and how the necessary very dense star clusters are formed.

Finally a class of models involve SMBHs forming from the remnants of Pop III stars, i.e., those forming from es-

entially metal-free gas with compositions set by big bang nucleosynthesis (see, e.g., Bromm 2013 for a review). McKee & Tan (2008) distinguished two classes of Pop III stars. Pop III.1 are those that form in isolation, i.e., without suffering significant influence from any other astrophysical source (i.e., other stars or SMBHs). Molecular hydrogen cooling leads to  $\sim 200 \text{K}$  temperatures in the centers of minihalos and first unstable fragment scales of  $\sim 100 M_\odot$  (Bromm et al. 2002; Abel et al. 2002). Pop III.2 stars still have primordial composition, but are influenced by external astrophysical sources, with the most important effects expected to be due to radiation feedback from ionizing or dissociating radiation (e.g., Whalen et al. 2008). One effect is to photoevaporate the gas from the minihalos, thus delaying star formation until the halos are more massive. The masses of Pop III.2 stars are thought to be potentially smaller than those of Pop III.1 stars due to enhanced electron fractions in gas that has suffered greater degrees of shock heating and/or irradiation that then promotes greater rates of  $\text{H}_2$  and HD formation and thus more efficient cooling and fragmentation (e.g., Greif & Bromm 2006).

However, although the initial unstable baryonic mass scale is commonly thought to be  $\sim 100 M_\odot$  in Pop III.1 halos set by the microphysics of  $\text{H}_2$  cooling, the ultimate masses of the stars that form are quite uncertain. The initial  $\sim 100 M_\odot$  unstable “core” is typically located at the center of the dark matter minihalo and surrounded by an envelope of  $\sim 10^5 M_\odot$  of gas that is bound to the halo. Tan & McKee (2004) and McKee & Tan (2008) presented semi-analytic estimates for final accreted masses of Pop III.1 protostars of  $\sim 140 M_\odot$  set by disk photoevaporation feedback. Using improved protostellar evolution models, Tanaka, Tan & Zhang (2017) have revised these estimates to  $\sim 50 M_\odot$ . Hosokawa et al. (2011) found similar results using radiation-hydrodynamic simulations. Tan, Smith & O’Shea (2010) applied the MT08 model to accretion conditions in 12 minihalos from the simulations of O’Shea et al. (2006), i.e., that have a variety of accretion rates, and estimated an initial mass function that peaked at  $\sim 100 M_\odot$  with a tail extending to  $\sim 10^3 M_\odot$  from those sources that have the highest accretion rates. Hirano et al. (2014) and Susa et al. (2014) presented radiation-hydrodynamic simulations of populations of  $\sim 100$  Pop III.1 stars, deriving initial mass functions peaking from  $\sim 10$ – $100 M_\odot$ , with a tail out to  $\sim 10^3 M_\odot$ . Their formation redshifts extended from  $z \sim 35$  down to  $z \sim 10$ .

While the above estimates for Pop III.1 masses are certainly top heavy compared to present-day star formation, they are still relatively low compared to the masses of SMBHs. To reach  $\sim 10^9 M_\odot$  in a few hundred Myr to explain the observed high- $z$  quasars would require near continuous maximal (Eddington-limited) accretion. Such accretion seems unlikely given that massive Pop III.1 stars would disrupt the gas in their natal environments by radiative and mechanical feedback (e.g., O’Shea et al. 2005; Johnson & Bromm 2007; Milosavljević et al. 2009).

Several authors have invoked the effect of coherent relative streaming velocities between dark matter and gas (Tsaliakhovich & Hirata 2010), which then leads to more massive (on average by about a factor of 3; Greif et al. 2011b; see also Fialkov et al. 2012 and Schauer et al. 2017) minihalos being the sites of Pop III.1 star formation, as a mechanism that may lead to conditions of SMBH formation. The

idea is that in the rarer cases where a minihalo is forming in a region where the streaming velocities are significantly ( $\gtrsim 2\times$ ) larger than average, then the minihalo mass at time of first star formation is also larger, perhaps  $\sim 10^7 M_\odot$  with a virial temperature  $\sim 8,000\text{K}$  (Tanaka & Li 2014). Collapse in such a halo would proceed at a relatively high accretion rate that can lead to protostellar swelling (Hosokawa et al. 2016) that reduces ionizing feedback. Simulations of such a model to form a  $34,000 M_\odot$  protostar have been presented by Hirano et al. (2017). This mechanism is potentially attractive, especially since it is relatively simple in being able to predict the formation locations of the sites of SMBH formation (Tanaka & Li 2014). However, whether or not this mechanism can produce sufficient numbers of SMBHs and whether a minimum characteristic mass of  $\sim 10^5 M_\odot$  can naturally be produced, rather than a continuous distribution with large numbers of IMBHs, remains to be determined.

In the next subsection we discuss how the outcome of Pop III.1 star formation may be altered under the influence of the energy input from Weakly Interacting Massive Particle (WIMP) dark matter self-annihilation. This mechanism may provide a route for the formation of supermassive, i.e.,  $\sim 10^5 M_\odot$ , Pop III.1 stars, which would then collapse to form SMBHs. Furthermore, this mechanism, which requires special conditions of the co-location of the protostar with the central density cusp of the dark matter halo, is only expected to be possible in Pop III.1 sources. This opens up the possibility of a “bifurcation” in the collapse outcome, i.e.,  $\sim 10^5 M_\odot$  SMBHs from Pop III.1 sources and  $\lesssim 100 M_\odot$  stellar populations from all other sources. Another attractive feature of this scenario for SMBH formation is its relative simplicity, with relatively few free parameters. It is thus amenable to incorporation into semi-analytic models of structure and galaxy formation to make testable predictions.

### 1.3 Population III.1 Dark Matter Annihilation Powered Protostars as SMBH Progenitors

One potential mechanism that may allow supermassive Pop III.1 stars to form is energy injection inside the protostar (i.e., during the accretion phase) by WIMP dark matter self-annihilation (Spolyar et al. 2008; Natarajan, Tan & O’Shea 2009, hereafter NTO09). As discussed below, this energy injection can be sufficient to support the protostar in a very large, swollen state, which gives it a relatively cool photospheric temperature and thus relatively weak ionizing feedback. If this state of weak feedback can be maintained as the protostar accretes the baryonic content of its minihalo, i.e.,  $\sim 10^5 M_\odot$ , then this provides a pathway to create a supermassive star, which would be expected to soon collapse to a SMBH.

NTO09 estimated that for the early phases of protostellar evolution to be significantly affected by WIMP annihilation heating, the WIMP mass needs to be  $m_\chi \lesssim$  several  $\times 100$  GeV, based on the size of the initial protostellar core in which WIMP heating dominated over baryonic cooling. Such WIMP masses are consistent with constraints on  $m_\chi$  that are based on constraints on the WIMP annihilation cross section along with the requirement that the actual cross section should equal the thermal relic value of  $\sim 3 \times 10^{-26} \text{cm}^3 \text{s}^{-1}$  (i.e., that necessary for all, or most, dark

matter to be composed of WIMPs). For example, from particle production in colliders, Khachatryan et al. (2016) find  $m_\chi \gtrsim 6$  to  $30$  GeV depending on whether the process is mediated via vector or axial-vector couplings of Dirac fermion dark matter. From indirect searches via Fermi-LAT observations of expected gamma ray emission from 15 Milky Way dwarf spheroidal satellite galaxies, including assumptions for modeling their dark matter density structures, Ackermann et al. (2015) report  $m_\chi \gtrsim 100$  GeV for WIMPs annihilating via quark and  $\tau$ -lepton channels. Such results suggest there may be only a relatively narrow range of WIMP masses that are viable for this scenario of dark matter powered Pop III.1 protostars.

Also, direct detection experiments that constrain (spin dependent and independent) WIMP-nucleon elastic scattering cross sections have yet to detect signatures of WIMP dark matter (e.g., Agnese et al. 2014; Akerib et al. 2016). While these results do not provide a firm constraint on the value of  $m_\chi$ , they do have implications for the ability Pop III.1 protostars to capture WIMPs of a given mass via such scattering interactions.

Spolyar et al. (2009) followed the growth of Pop III.1 protostars including the effects of annihilation heating from their initial and captured dark matter. We note that such dark matter powered protostars are objects that collapse to densities quite similar to those of normal protostars: e.g., for the initial model considered by Spolyar et al. (2009), which has  $3 M_\odot$  and soon achieves a radius of  $\sim 3 \times 10^{13}$  cm, i.e.,  $\sim 2$  AU, the central densities are  $n_{\text{H,c}} \sim 6 \times 10^{17} \text{cm}^{-3}$  and the mean densities  $\bar{n}_{\text{H}} \sim 3 \times 10^{16} \text{cm}^{-3}$ . In their canonical case without captured WIMPs, collapse of the protostar to the main sequence was delayed until about  $800 M_\odot$ . They also considered a “minimal capture” case with background dark matter density of  $\rho_\chi = 1.42 \times 10^{10} \text{GeV cm}^{-3}$  and  $\sigma_{\text{sc}} = 10^{-39} \text{cm}^2$  (for spin-dependent scattering relevant to H) that results in about half the luminosity being from annihilation of captured WIMPs (with  $m_\chi = 100$  GeV) and the other half from nuclear fusion at the time the protostar joins the main sequence. The results from Akerib et al. (2016) imply  $\sigma_{\text{sc}} \lesssim 5 \times 10^{-39} \text{cm}^2$ . However, more recent studies have lowered this to  $\sigma_{\text{sc}} \lesssim 8 \times 10^{-40} \text{cm}^2$  (Akerib et al. 2017) and  $\sigma_{\text{sc}} \lesssim 5 \times 10^{-41} \text{cm}^2$  for a WIMP mass of 100 GeV, which thus call into question the validity of the minimal capture model and require consideration of other capture models.

Freese et al. (2010) and Rindler-Daller et al. (2015) have presented models of protostellar evolution of dark matter annihilation powered protostars that continue to accrete to much higher masses. In the study of Rindler-Daller et al., starting with initial protostellar masses from 2 to  $5 M_\odot$ , the protostars are followed to  $\gtrsim 10^5 M_\odot$  for cases with accretion rates of  $10^{-3}$  and  $10^{-1} M_\odot \text{yr}^{-1}$  and WIMP masses of  $m_\chi = 10, 100, 1000$  GeV. While feedback effects, i.e., ionization, are not considered that may limit the accretion rate, the protostars tend to remain relatively large and thus cool, especially for the  $m_\chi = 10$  and 100 GeV cases.

The requirements for forming supermassive Pop III.1 protostars, which then collapse to form SMBHs, can be summarized as follows. The ionizing luminosity needs to remain low compared to that of a protostar of the equivalent mass on the zero age main sequence (ZAMS), else disk photoevaporation (McKee & Tan 2008; Hosokawa et al. 2011; Tanaka et al. 2017) will shut off the accretion flow. There appear to

be a range of models for  $m_\chi \lesssim 1$  TeV in which this occurs, which could allow continued accretion of the baryons within the minihalo, in principle up to the entire baryonic content  $\sim 10^5 M_\odot$  (Rindler-Daller et al. 2015). Indeed, efficient accretion of the gas of the minihalo to the central protostar is a requirement and feature of this model. For this to occur, additional requirements are that angular momentum can be lost from the gas and that fragmentation does not occur to create gravitational fluctuations that scatter and thus dilute the central dark matter density or divert a significant fraction of the baryonic mass flux of the collapsing minihalo to a binary companion or multiple companions. Especially binary formation that leads to displacement of the primary star from the “central region” of the dark matter halo could then shut off continued capture of dark matter to the protostar, which may be necessary to achieve the highest masses.

The question of angular momentum transport is one that has already been studied in the context of traditional models and simulations of Pop III.1 star formation. Abel, Bryan & Norman (2002) showed that the specific angular momentum of the gas as a function of radius in the minihalo maintained a fairly constant, sub-Keplerian level during the early phases of infall. Significant angular momentum transport was achieved by trans-sonic turbulent motions, driven by the gravitational contraction. A key feature of this infall is that it occurs relatively slowly, mediated by the relatively weak rates of H<sub>2</sub> ro-vibrational line cooling, so the gas in the minihalo is in approximate pressure and virial equilibrium. This allows sufficient time for angular momentum transport within the gas cloud.

At later stages of collapse, after the first Pop III.1 protostar has formed, WIMP annihilation heating is only expected to be significant in the protostar if these objects are co-located near the peaks of their natal dark matter minihalos and the dark matter density stays sufficiently high in these zones.

Spolyar et al. (2009) have presented a case in which effective WIMP annihilation heating alters the evolution of the protostar for a dark matter density of  $\rho_\chi \gtrsim 10^{10}$  GeV cm<sup>-3</sup>. For the three example minihalos considered by NTO09, the initial radii defining such a central region are 72, 45 and 89 AU. Stacy et al. (2014) carried out a simulation that followed Pop III.1 star formation including an “active” dark matter halo that has its central density reduced by interactions with a clumpy accretion disk around the primary protostar. The radius of the zone that has  $\rho_\chi \gtrsim 10^{10}$  GeV cm<sup>-3</sup> was still  $\sim 40$  AU at the end of their simulation, 5000 yr after first protostar formation, and the primary protostar was located within this zone.

In terms of fragmentation of the gas, this was seen to be relatively limited during the initial phases of collapse of minihalos in the cosmological simulations of Turk, Abel & O’Shea (2009): about 80% of their minihalos appear to collapse to a single protostellar “core,” i.e., the self-gravitating gas in which a single rotationally supported disk will form. However, a number of authors have claimed that later fragmentation of the primary protostar’s accretion disk may lead to formation of multiple lower mass stars leading to either formation of a close binary or even a cluster of low-mass Pop III stars. Clark et al. (2011) followed the evolution to about 110 yr after first protostar formation, including effects of protostellar heating on the disk. By this time the protostar

had accreted almost  $0.6 M_\odot$ . It still resided near the center of its accretion disk, which, being gravitationally unstable, had also formed three lower mass ( $\lesssim 0.15 M_\odot$ ) protostars. Greif et al. (2011a) followed the collapse and fragmentation of five different minihalos to about 1000 yr after first protostar formation, by which time masses of several solar masses had been achieved. They typically observed several tens of protostars forming by fragmentation in the main accretion disk, although describe that most are likely susceptible to merging with the primary protostar (a process they could not follow in their simulations).

Smith et al. (2012) carried out similar simulations, but now including the effects of WIMP annihilation on the chemistry and thermodynamics of the collapse. They found much reduced fragmentation: in one case only a single, primary protostar formed; in another, just one secondary protostar. The primary protostars reached  $\gtrsim 10 M_\odot$  and remained in the central regions of their host minihalos, which would imply there could be an important effect on subsequent protostellar evolution due to WIMP annihilation heating. Stacy et al. (2014) also carried out such simulations, but now with no protostellar heating feedback. They formed a primary protostar that reached  $8 M_\odot$  after 5000 yr along with several lower-mass companions. This primary protostar was still located in a zone with dark matter density  $\rho_\chi \gtrsim 10^{10}$  GeV cm<sup>-3</sup>.

Another point that should be noted is that the propensity of protostellar accretion disks to fragment will also depend on the magnetic field strength in the disk and none of the above fragmentation studies have included  $B$ -fields. Dynamo amplification of weak seed fields that arise via the Biermann battery mechanism may occur in turbulent protostellar disks: see, e.g., Tan & Blackman (2004); Schleicher et al. (2010); Schober et al. (2012); Latif & Schleicher (2016). These studies all predict that dynamically important, near equipartition  $B$ -fields will arise in Pop III protostellar disks. From numerical simulations of local star formation it is well known that such  $B$ -fields are important for enhancing transport of angular momentum during collapse and also for generally acting to suppress fragmentation compared to the unmagnetized case (e.g., Price & Bate 2007; Hennebelle et al. 2011). Magnetic fields would similarly be expected to reduce the density fluctuations in the accretion disks and the size of the disks, which would then reduce the amount of gravitational interaction that is seen to dilute the dark matter density cusp in the simulation of Stacy et al. (2014). If early fragmentation is suppressed then this may allow the primary protostar to achieve a significant mass and luminosity so that its radiative feedback then later becomes the dominant means of limiting fragmentation.

In summary, whether or not a single dominant, centrally-located protostar is the typical outcome of collapse of Pop III.1 minihalos is still uncertain. Such outcomes are seen in some pure hydrodynamic simulations of collapse, especially when the effects of dark matter annihilation heating are included. If magnetic fields can be amplified to near equipartition by an accretion disk dynamo, then this outcome is expected to be even more likely to occur.

On the other hand, Pop III.2 stars, if formed in a minihalo that undergoes very significant early stage fragmentation to multiple “cores,” are not generally expected to be co-located with the dark matter density peak. Co-location

will also not occur for stars forming in more massive halos, where first atomic cooling and then H<sub>2</sub> or metal or dust cooling allows formation of a large-scale rotationally-supported thin disk, which then fragments to form a more normal stellar population, i.e., the early stages of a galactic disk.

We thus regard formation of dark matter powered Pop III.1 stars as a potentially attractive mechanism to explain the origin of SMBHs, possibly all SMBHs. If the protostar is in a large, swollen state, as is generally expected if WIMP annihilation heating is important, and is thus able to accrete a significant fraction of the initial baryonic content of the Pop III.1 minihalo, i.e.,  $\gtrsim 10^5 M_\odot$ ,

then this is likely to lead to SMBH formation via an intermediate stage of supermassive star formation. Collapse to a SMBH may be induced by the star becoming unstable with respect to the general relativistic radial instability (GRRI). For nonrotating main sequence stars this is expected to occur at a mass of  $\simeq 5 \times 10^4 M_\odot$  (Chandrasekhar 1964), while in the case of maximal uniform rotation this is raised to  $\sim 10^6 M_\odot$  (Baumgarte & Shapiro 1999).

SMBH formation from supermassive Pop III.1 stars that efficiently accrete the baryons from their minihalos is thus a mechanism that can help explain the apparent absence or dearth of SMBHs with masses  $\lesssim 10^5 M_\odot$ . This lower limit to the masses of SMBHs is not easily explained in most other formation models.

#### 1.4 Goals and Outline of this Paper

Our goals in this paper are to make predictions for cosmological populations of SMBHs that form via Pop III.1 protostars supported by dark matter annihilation heating. We note that a broad consensus on the validity of this mechanism as an outcome of Pop III.1 star formation has not yet been reached (see, e.g., Clark et al. 2011; Greif et al. 2011a; Smith et al. 2012; Stacy et al. 2014). However, here we will assume the validity of this model in order to follow its consequences and predictions. Such predictions, especially the formation history of Pop III.1 stars, the overall number densities of these stars and their proposed SMBH remnants, and their clustering properties, are necessary as a first step to eventually connect to observations of SMBH populations at high and low redshift and thus test this theoretical model of SMBH formation.

The conditions needed to be a Pop III.1 protostar, i.e., for being “undisturbed” by other astrophysical sources, so that the protostar is co-located with the dark matter cusp to enable effective WIMP annihilation heating, are uncertain. This is because the radiative influence on a halo from a neighboring source and its effect on subsequent star formation is a very complicated problem (e.g., Whalen & Norman 2006), which also depends on the nature of the sources of feedback. For simplicity we will therefore first parameterize the required “isolation distance,”  $d_{\text{iso}}$ , that is needed for a given halo to be a Pop III.1 source and consider a range of values.

The outline of the paper is as follows. In §2 we present our methods for simulating structure formation and identifying Pop III.1 minihalos. In §3 we present our main results, i.e., the evolution of the number densities of Pop III.1 stars and SMBH remnants (§3.1), the sensitivity of the results to cosmic variance and the cosmological parameter  $\sigma_8$  (§3.2),

the mass function of SMBH host halos in the post formation phase at  $z = 10$  and  $15$  (§3.3), synthetic sky maps of the sources (§3.4), and evaluation of the angular correlation function of the predicted SMBH populations in (§3.5).

We discuss the implications of our results and draw conclusions in §4.

## 2 METHODS

We utilize PINOCCHIO (PINpointing Orbit Crossing Collapsed Hierarchy Objects), which is a code based on Lagrangian Perturbation Theory (LPT) (Moutarde et al. 1991; Buchert & Ehlers 1993; Catelan 1995)

for the fast generation of catalogs of dark matter halos in cosmological volumes. LPT (see review by Monaco 2016) is a perturbative approach to the evolution of overdensities in a matter-dominated Universe. It is based on the Lagrangian description of fluid dynamics, and its validity is mainly limited to laminar flows, where the orbits of mass elements do not cross. As such, this is ideal to describe the early universe, characterised by a limited degree of non-linearity. Starting from a realization of a Gaussian density field in a box sampled by  $N^3$  particles,

using an ellipsoidal collapse model, PINOCCHIO computes the time at which each particle is expected to suffer gravitational collapse (i.e., “orbit crossing,” when the map from initial, Lagrangian, to final, Eulerian positions becomes multivalued), then collects the collapsed particles into halos with an algorithm that mimics their hierarchical clustering. The result is a catalog of dark matter halos with known mass, position, velocity and merger history.

The code was introduced in its original form by Monaco, Theuns & Taffoni (2002),

where it was demonstrated that it can accurately reproduce “Lagrangian” quantities like halo masses and merger histories. This was later confirmed by other groups (see the review in Monaco et al. 2013).

A massively parallel version was presented by Monaco et al. (2013)

and extended and tested by Munari et al. (2016).

We have compared the mass function of halos produced by our PINOCCHIO simulations with the analytic fit to the N-body simulations of Reed et al (2007), finding generally very good agreement, but with two caveats. First, at  $z = 30$ , while the number of minihalos of mass  $\sim 10^6 M_\odot$  predicted by PINOCCHIO agrees to within  $\sim 20\%$  with the Reed et al. results, there is a modest deficit of higher-mass halos by about a factor of 2, potentially caused by finite volume effects (see Reed et al. 2007; Monaco 2016). For the purposes of this paper, we are primarily concerned with predicting the emergence of minihalos and so consider the results of PINOCCHIO to be sufficiently accurate for such purposes. Second, at  $z = 10$  there is a mild overestimate of  $\gtrsim 10^8 M_\odot$  halos by about a factor of 1.5, due to the fact that the PINOCCHIO mass function has been calibrated on the numerical fit of Watson et al. (2014), which gives more massive halos in the high mass tail. These discrepancies give a measure of the uncertainties in our numerical halo mass function estimates.

For clustering properties, Munari et al. (2016) showed how PINOCCHIO’s prediction of the clustering of halos

improves when higher orders of LPT are used. As a result, clustering in  $k$ -space is well reproduced, to within a few per cent, up to a wavenumber of at least  $k = 0.3 h \text{ Mpc}^{-1} = 0.203 h_{0.68} \text{ Mpc}^{-1}$ , where  $h_{0.68} \equiv h/0.6774 = 1$  is the normalized Hubble parameter and will be used in lieu of  $h$  henceforth. A degradation of quality is seen at  $z < 0.5$ , where the density field becomes significantly non-linear. Clustering in configuration space is very well reproduced on comoving scales larger than  $\sim (10 - 20)h^{-1} \text{ Mpc} = (14.76 - 29.52)h_{0.68}^{-1} \text{ Mpc}$ .

In this paper we use the latest code version with 2LPT (2nd order) displacements, that give a very good reproduction of clustering while keeping memory requirements to  $\sim 150$  bytes per particle, thus allowing running of large boxes (3LPT would require nearly twice as much memory). PINOCCHIO is well-suited to the study of the formation of first stars and SMBHs from high- $z$ , relatively low-mass halos spanning large cosmological volumes.

Adopting a standard Planck cosmology:  $\Omega_m = 0.3089$ ,  $\Omega_\Lambda = 0.6911$ ,  $n_s = 0.9667$ ,  $\sigma_8 = 0.8159$ ,  $\Omega_b h^2 = 0.02230 = \Omega_b h_{0.68}^2 = 0.0102$ ,  $w_0 = -1$ ,  $w_1 = 0$  (Planck collaboration 2015), we simulate a  $40.96 h^{-1} = 60.47 h_{0.68}^{-1} \text{ Mpc}$  comoving cubical box sampled with  $4096^3$  particles, thus reaching a particle mass of  $1.2 \times 10^5 M_\odot$ . This allows us to sample a  $10^6 M_\odot$  halo with  $\sim 10$  particles.

We first run the simulation down to redshift of 15. This required 10 Pb of RAM and took less than an hour on 1376 cores of the GALILEO@CINECA machine, most of the time being spent in writing 211 outputs from  $z = 40$  to  $z = 10$  in redshift steps of  $\Delta z = 0.1$ . We then continued the simulation down to  $z = 10$ , outputting in steps of  $\Delta z = 1$ . This is the largest PINOCCHIO run ever presented in a paper.

From the simulation outputs, we identify halos that form Pop III.1 stars by looking for minihalos with masses just crossing a threshold of  $10^6 M_\odot$ , which are also isolated from any other existing minihalos (i.e., that may host Pop III.1, Pop III.2 or Pop II sources) by a proper distance of  $d_{\text{iso}}$ . This assumption of a constant threshold halo mass of  $10^6 M_\odot$  is motivated first by its simplicity. The masses of the dark matter halos of the  $\sim 100$  Pop III stars studied in the simulations of Hirano et al. (2014), have a fairly narrow mass distribution around  $\sim 3 \times 10^5 M_\odot$ . However, the effect of coherent relative streaming velocities between dark matter and gas (Tselikhovich & Hirata 2010) have been shown to delay Pop III star formation, i.e., increasing the required halo mass by about a factor of three (Greif et al. 2011b), which was not allowed for in the study of Hirano et al. (2014). Given these considerations, we regard the choice of a constant threshold mass of  $10^6 M_\odot$  as a reasonable first approximation. However, we have also explored the effects of varying this choice of threshold mass up to values of  $4 \times 10^6 M_\odot$ , which, as we describe below, only have very minor effects on our main results.

On the other hand, the main parameter that we explore in this model of SMBH formation from Pop III.1 sources is the isolation distance,  $d_{\text{iso}}$ , with values of  $d_{\text{iso}} = 10, 20, 30, 50, 100, 300 \text{ kpc}$  being considered.

Once halos have been tagged as being Pop III.1 sources we then track their subsequent evolution. First, for the next period of time,  $t_{*f}$ , they are considered to be ‘‘Pop III.1 Stars’’, which includes the protostellar accretion phase and any additional period of stellar evolution. We examine spe-

cific choices of  $t_{*f} = 10, 30$  and  $100 \text{ Myr}$ . For  $10^5 M_\odot$  stars that have negligible post accretion lifetimes, i.e., if accreting right up to the point of GRRI, this corresponds to average accretion rates in the range  $10^{-3}$  to  $10^{-2} M_\odot \text{ yr}^{-1}$ , which are typical values expected for such sources (e.g., Tan & McKee 2004; Tan et al. 2010; see also the pre-feedback accretion rates in the simulations of Hirano et al. 2014).

After  $t_{*f}$ , Pop III.1 stars are assumed to collapse into SMBH remnants. We note that while the value of  $t_{*f}$  is quite uncertain, it does not affect the eventual properties of the SMBH remnants. The halos containing SMBHs are tracked down to  $z = 10$ . These halos grow in mass by both accretion of dark matter particles (i.e., sub-minihalos) and by mergers with already identified minihalos and larger halos. During a merger of two halos, the more massive halo retains its identity and typically the SMBH will be occupying the more massive of the two merging halos. Occasionally the SMBH and its host halo merge with a more massive halo, in which case the presence of the SMBH is transferred to this new halo. Sometimes two merging halos will each already host a SMBH: this situation is expected to lead to SMBH-SMBH binary in the center of the new halo and thus potentially a merger of the two black holes.

In this paper we focus on SMBH locations, number densities and host halo properties, and defer modeling of SMBH growth due to gas accretion (i.e., active galactic nuclei) to a future paper. While we note when SMBH mergers are expected to occur, we also defer analysis of these merger properties and potential gravitational wave signatures to a future study.

### 3 RESULTS

We applied the algorithm described in §2 to identify Pop III.1 minihalos and follow their assumed SMBH remnants down to  $z = 10$  for the fiducial simulation volume and several other test volumes. The main results for SMBH formation histories, halo properties and clustering properties are described in this section.

#### 3.1 Cosmic Evolution of the Number Density of Pop III.1 Stars and SMBHs

Figure 1 shows the redshift evolution of the comoving total number density,  $n$ , of Pop III.1 stars and remnants (i.e., assumed in this model to be SMBHs) for different values of  $d_{\text{iso}}$  ranging from 10 to 300 kpc (proper distances). As we will see below, for the assumption of 10 to 100 Myr lifetimes of Pop III.1 stars, these totals soon become dominated by the SMBH remnants. Within this simulated  $(60.47 h_{0.68}^{-1} \text{ Mpc})^3$  comoving volume, Pop III.1 stars start forming just after  $z = 40$ . For large values of  $d_{\text{iso}}$ , the number of new Pop III.1 sources that are able to form decreases more quickly and  $n$  asymptotes to a constant value. For example, for  $d_{\text{iso}} = 100 \text{ kpc}$  Pop III.1 stars have largely ceased to form by  $z \sim 25$ , while for  $d_{\text{iso}} = 10 \text{ kpc}$  they continue to form still at  $z = 10$ .

Comparison of the number density of sources formed in these models with the present day ( $z = 0$ ) number density of SMBHs,  $n_{\text{SMBH}}$ , constrains  $d_{\text{iso}}$ . We estimate  $n_{\text{SMBH}}(z =$

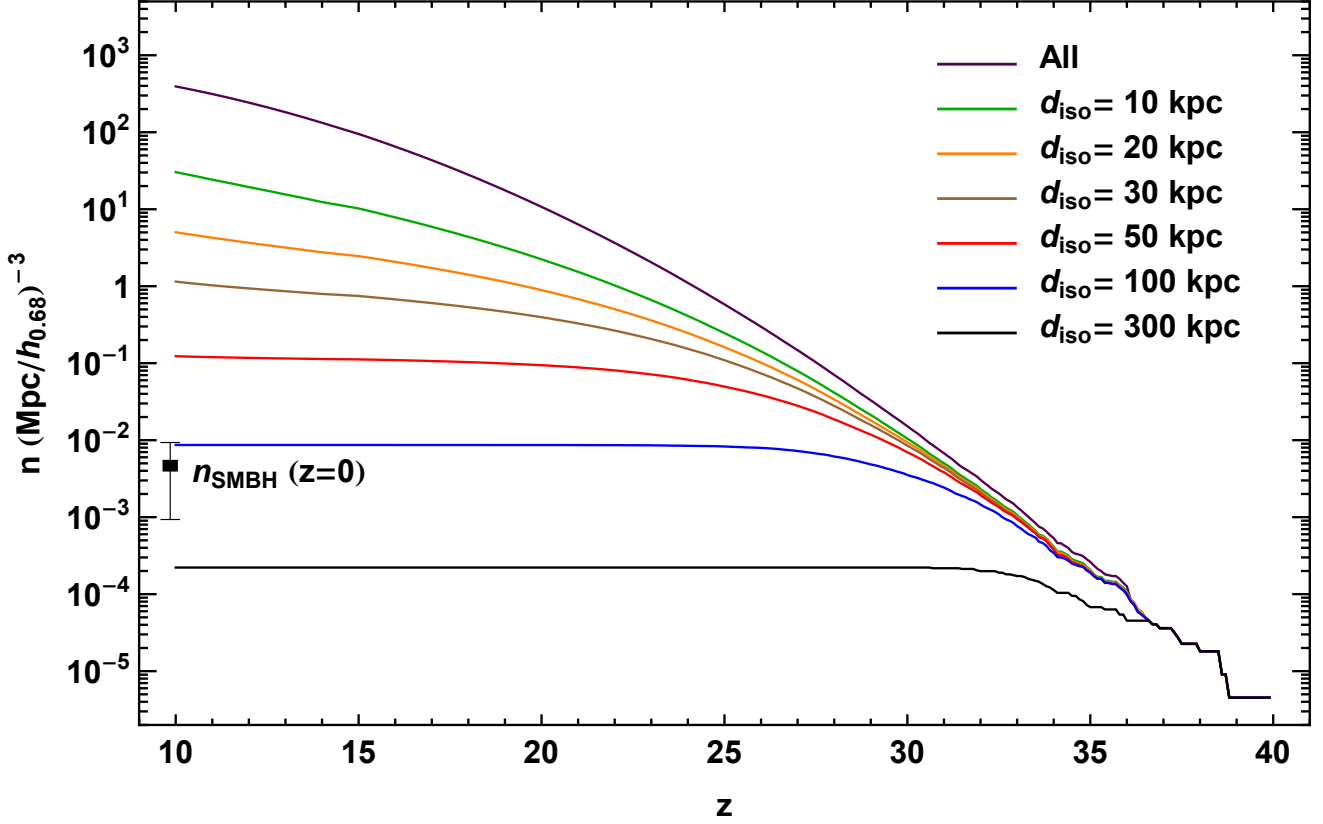


**Figure 1.** Evolution of comoving total number density of Pop III.1 stars and their SMBH remnants for different values of  $d_{\text{iso}}$  ranging from 10 to 300 kpc (proper distances). The number density of all dark matter halos with  $M > 10^6 M_{\odot}$  is also shown for reference. The data point  $n_{\text{SMBH}}(z=0)$  drawn schematically on the left side of the figure shows an estimate for the present day number density of SMBHs assuming one SMBH is present in all galaxies with  $L > L_{\text{min}}$ . The solid square shows this estimate for  $L_{\text{min}} = 0.33L_*$ , while the lower and upper bounds assume  $L_{\text{min}} = 0.1L_*$  and  $L_*$ , respectively.

0)  $\sim 0.015 (\text{Mpc}/h)^{-3} = 4.6 \times 10^{-3} (\text{Mpc}/h_{0.68})^{-3}$  by assuming that all galaxies with  $L_{\text{min}} > 0.33L_*$  host SMBHs and integrating over the local galaxy luminosity function assumed to be a Schechter function of the form

$$\phi(L) = \left(\frac{\phi^*}{L^*}\right) \left(\frac{L}{L^*}\right)^{\alpha} e^{-(L/L^*)} \quad (1)$$

where  $\phi^* = 1.6 \times 10^{-2} (\text{Mpc}/h)^{-3} = 4.9 \times 10^{-3} (\text{Mpc}/h_{0.68})^{-3}$  is the normalization density and  $L^*$  is the characteristic luminosity corresponding to  $M_{\text{B}} = -19.7 + 5 \log h = -20.55$  (e.g., Norberg et al. 2002) and  $\alpha \simeq 1.2$  is the power law slope at low  $L$ . This value is shown on the left edge of Figure 1, with the error bar resulting from assuming  $L_{\text{min}} = 0.1$  to  $1 L_*$ , i.e., a range from  $9.3 \times 10^{-3} (\text{Mpc}/h_{0.68})^{-3}$  to  $9.3 \times 10^{-4} (\text{Mpc}/h_{0.68})^{-3}$ . For comparison, integrating the SMBH mass function from Vika et al. (2009), we estimate the number density of SMBHs to be  $8.79 \times 10^{-3} (\text{Mpc}/h_{0.68})^{-3}$ , which is consistent with our more simplistic estimate.

Note when comparing with  $n_{\text{SMBH}}(z=0)$  that the model  $n$  does not account for any decrease due to merging of SMBHs. However, we can assess how many mergers occur in the simulation: for  $d_{\text{iso}} = 50$  kpc only  $\sim 0.2\%$  of SMBHs suffer a merger with another SMBH by  $z = 10$ , i.e., it is a very minor effect. Some additional SMBH mergers will occur at  $z < 10$ , but given the low rate of merging at  $z > 10$  and the low fraction of  $> 10^9 M_{\odot}$  halos at  $z = 10$  that host SMBHs (for  $d_{\text{iso}} = 50$  kpc this is  $\simeq 0.16$ , discussed below), it seems unlikely that this will lead to more than a factor of three reduction in  $n$ . Thus we consider that the cases of  $d_{\text{iso}} = 50$  and 100 kpc are the most relevant in the context of this model of Pop III.1 seeds for forming the whole cosmic population of SMBHs. From here on we will focus on the cases between  $d_{\text{iso}} = 30$  and 300 kpc.

If we assume SMBH mergers are negligible, then we can use the asymptotic (i.e.,  $z = 10$ ) number density of SMBH remnants for the cases of  $d_{\text{iso}} = 50$  to 300 kpc to estimate the range of  $d_{\text{iso}}$  that is implied by our adopted constraint



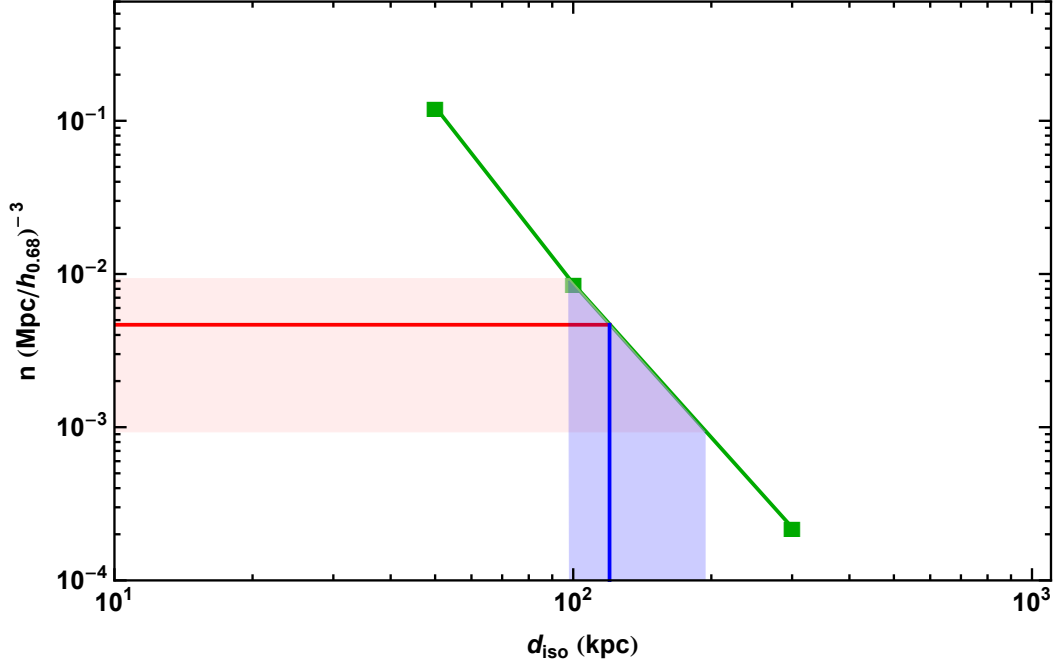


**Figure 2.** Asymptotic ( $z = 10$ ) number density of SMBHs,  $n$ , versus  $d_{\text{iso}}$ . The green squares show results for the analysis with  $d_{\text{iso}} = 30, 50$  and  $100$  kpc, joined by the green lines assuming a power law dependence of  $n$  on  $d_{\text{iso}}$ . The red line indicates  $n_{\text{SMBH}}(z = 0)$  corresponding to  $L_{\text{min}} = 0.33L_*$  and the red band shows the range of  $n_{\text{SMBH}}$  corresponding to  $L_{\text{min}} = 0.1$  to  $1 L_*$ . The blue line and band show the corresponding value and range of  $d_{\text{iso}}$  implied by this range of  $n$ .

on  $n_{\text{SMBH}}(z = 0)$ . This is shown in Figure 2 as a blue shaded band, i.e., implying  $100 \text{ kpc} \lesssim d_{\text{iso}} \lesssim 200 \text{ kpc}$ .

We have also checked the sensitivity of our results to the choice of  $1 \times 10^6 M_{\odot}$  as the threshold halo mass for leading to a Pop III.1 source. As discussed above in §1, effects such as dark matter particle streaming velocities relative to baryons may increase this threshold mass (e.g., Fialkov et al. 2012). However, we find that raising the threshold mass by a factor of four, i.e., to  $4 \times 10^6 M_{\odot}$ , has a very minor ( $\lesssim 20\%$ ) effect on the overall number density of the sources at late times, which is much smaller than the variation resulting from the choice of  $d_{\text{iso}}$ .

Figure 3 shows the separate evolution of the comoving number density of Pop III.1 stars, SMBH remnants and the total of these two components for  $d_{\text{iso}} = 30, 50, 100$  and  $300$  kpc for the case with  $t_{*f} = 10$  Myr. Pop III.1 stars dominate at very early times, while SMBHs dominate at later times. For example, for  $d_{\text{iso}} \sim 100$  kpc the Pop III.1 star formation rate (SFR) peaks at  $z \simeq 30$  and effectively stops below  $z \simeq 25$ , while for smaller values of  $d_{\text{iso}}$  there can still be significant new Pop III.1 sources forming or existing at  $z \sim 10$  to  $15$ . We have seen that from the overall number of SMBH remnants produced in comparison to observed local comoving number densities of SMBHs that the models with  $d_{\text{iso}} = 50$  and  $100$  kpc are the most relevant if all SMBHs are to form via Pop III.1 seeds. Thus in Figure 4 we focus on these two cases and explore the effect of varying the overall time that Pop III.1 stars exist (i.e., combining their formation and subsequent lifetime before collapsing to SMBHs),  $t_{*f}$ , with values explored of  $10, 30$  and  $100$  Myr. Extending the duration of the Pop III.1 Star phase causes them to be

present down to lower redshifts, but, in the context of our modeling, does not affect the final number density of the SMBH remnants. For  $d_{\text{iso}} = 50$  kpc and  $t_{*f} = 100$  Myr, significant number densities of Pop III.1 stars can be present down to  $z=10$ , but still at levels that are about a factor of 30 smaller than at the peak at  $z \sim 20$ . Variation in  $t_{*f}$  also affects the redshift when the first SMBHs, i.e., AGN, appear. For  $t_{*f} = 10$  Myr, SMBHs start appearing at  $z \sim 35$  and the populations are largely in place by  $z \sim 25$ . However, for  $t_{*f} = 100$  Myr, SMBHs do not appear until  $z \sim 20$ . Thus the detection or non-detection of Pop III.1 supermassive stars and/or accreting SMBHs at  $z \simeq 10$  to  $15$ , potentially possible with the *James Webb Space Telescope (JWST)* (Freese et al. 2010), could help to distinguish between these models.

### 3.2 Effects of Cosmic Variance and $\sigma_8$

We study how the results are affected by cosmic variance by running several simulations of smaller volumes of  $(10 h^{-1} \text{ Mpc})^3 = (14.76 h_{0.68}^{-1} \text{ Mpc})^3$  and  $(20 h^{-1} \text{ Mpc})^3 = (29.52 h_{0.68}^{-1} \text{ Mpc})^3$ . For each of these volumes, five independent simulations were run using different random seeds to generate the initial conditions. Figure 5 shows the results of these runs for the number density evolution of Pop III.1 stars and SMBH remnants for the case of  $d_{\text{iso}} = 100$  kpc. We see that while there is moderate variation in redshift of the first Pop III.1 source in each volume, the dispersion in the final number densities of sources (i.e., for  $z \lesssim 25$ ) in these simulations is very minor.

Halo number densities will depend on cosmological parameters. In particular, the number of rare objects is mostly

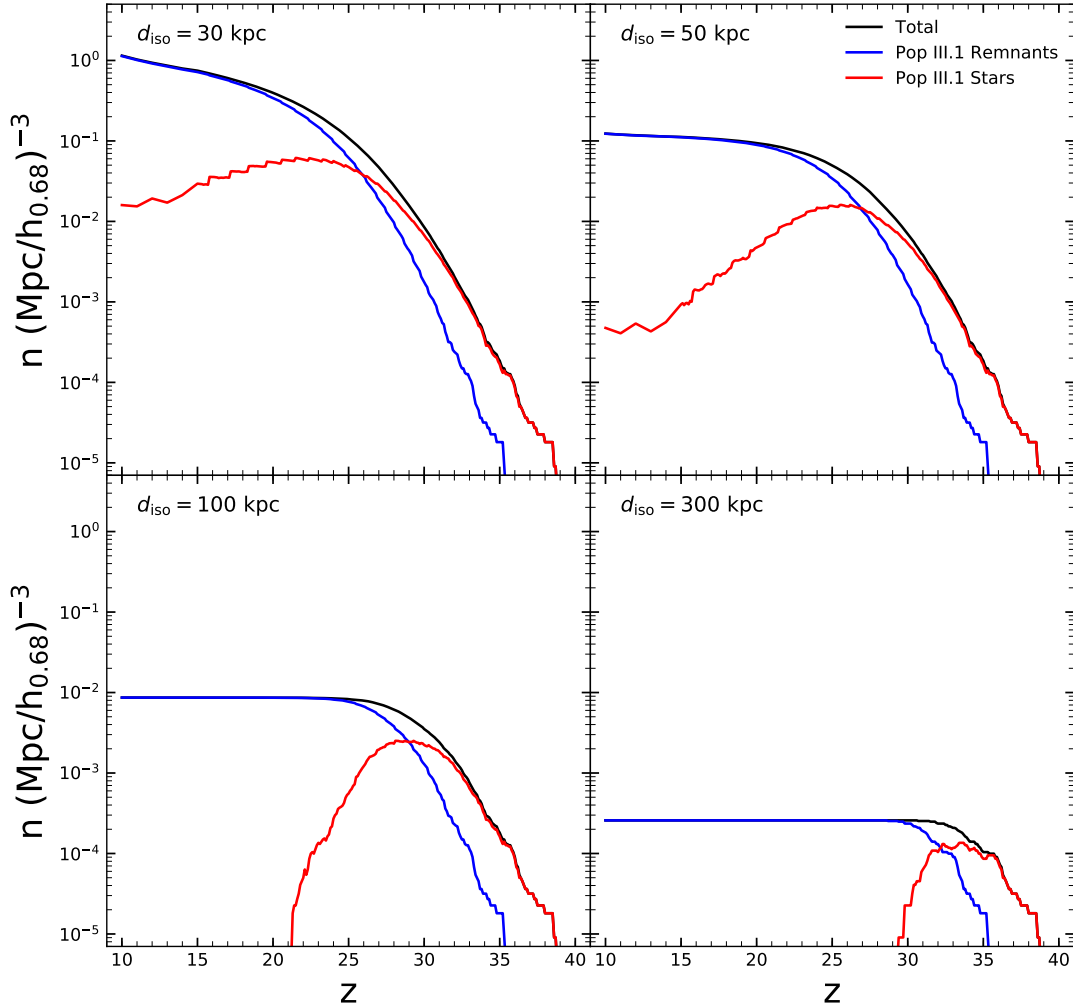


**Figure 3.** Evolution of the comoving number density of Pop III.1 stars (red lines), SMBH remnants (blue lines) and the total number of sources (black lines) for  $d_{\text{iso}} = 30$  kpc (top left), 50 kpc (top right), 100 kpc (bottom left) and 300 kpc (bottom right). All models shown here assume a Pop III.1 Star formation time and/or lifetime,  $t_{*f}$ , of 10 Myr.

sensitive to the normalization of the power spectrum via  $\sigma_8$ . Thus, next we examine how the choice of  $\sigma_8$  affects the number density of Pop III.1 stars and SMBHs. We explore a range of  $\sigma_8 = 0.830 \pm 0.015$  (Planck collaboration 2015). Figure 6 shows the effect of varying  $\sigma_8$  by this amount on the total number density of Pop III.1 stars and SMBHs for the case of  $d_{\text{iso}} = 100$  kpc for a simulation of a  $(29.52 h_{0.68}^{-1} \text{ Mpc})^3$  volume. Again the dispersion in the final number densities of sources (i.e., for  $z \lesssim 25$ ) in these simulations is very minor, i.e.,  $\lesssim 7\%$ .

### 3.3 Mass Function of SMBH-Host Halos

The halos that form Pop III.1 stars and host their SMBH remnants are then followed to lower redshifts, as far as  $z = 10$ . These halos grow in mass by accreting dark matter particles and merging with other identified halos. As described in §2, in a merger the more massive halo retains its identity. For values of  $d_{\text{iso}} \gtrsim 50$  kpc, the halos that are merging with the SMBH-hosting halos are typically of lower mass and do not host SMBHs. Occasionally, they are more massive, in which case the SMBH-hosting character of the halo is transferred to this new halo identity. Even more rare is a merger of two halos that both host SMBHs. The properties of these binary SMBH halos and predictions for the eventual

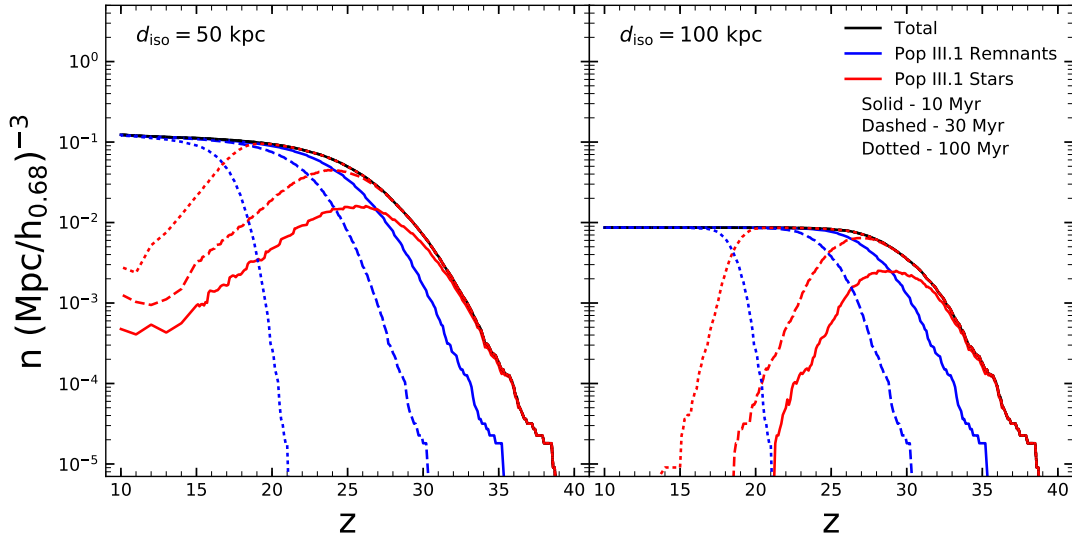


**Figure 4.** Effect of varying Pop III.1 star formation time and/or lifetime,  $t_{*f}$  on the evolution of the comoving number density of Pop III.1 stars (red lines), SMBH remnants (blue lines) and the total number of sources (black lines) for  $d_{\text{iso}} = 50$  kpc (left) and 100 kpc (right). Within each panel, different line styles of solid, dashed and dotted represent cases with  $t_{*f} = 10, 30, 100$  Myr, respectively.

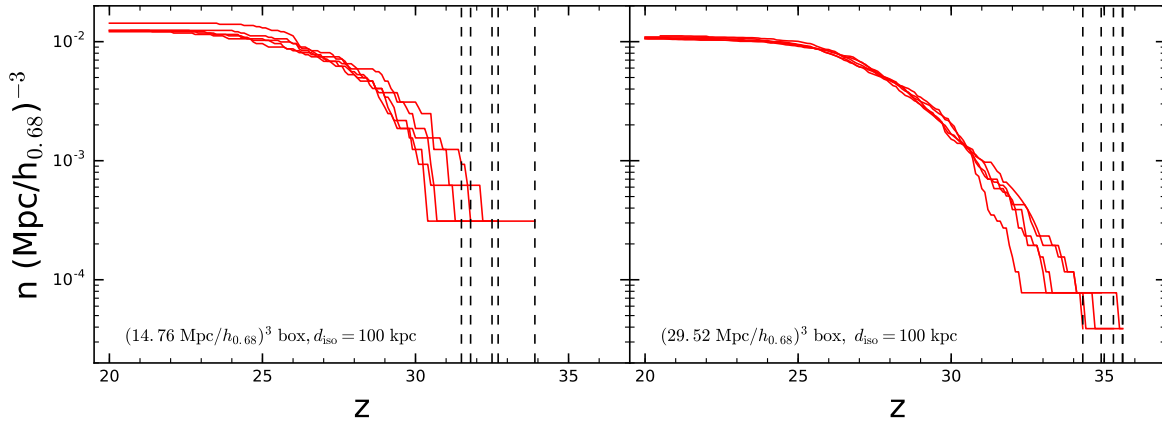


**Figure 5.** (a) *Left:* Evolution of the comoving total number density of Pop III.1 stars and their SMBH remnants for  $d_{\text{iso}} = 100$  kpc in five realizations of a  $(14.76 h_{0.68}^{-1} \text{ Mpc})^3$  volume. The vertical dashed lines indicate the redshift of the appearance of the first halo in each run. (b) *Right:* As (a), but now showing results for five realizations of a  $(29.52 h_{0.68}^{-1} \text{ Mpc})^3$  volume.

merger of the SMBHs will be presented in a future paper in this series. Here we focus simply on the mass function of the SMBH-hosting halos: Figure 7 shows the distribution of these masses at  $z = 10$  and  $15$  for cases of  $d_{\text{iso}} = 50$  and  $100$  kpc. For comparison, we also show the mass function of all halos at  $z = 15$  and  $10$  with dashed histograms.

For  $d_{\text{iso}} = 100$  kpc we see that at  $z = 15$  the typical SMBH-host halo has  $\gtrsim 10^7 M_{\odot}$ , while by  $z = 10$  this grows to  $\gtrsim 10^8 M_{\odot}$  (although note there can be some SMBHs in lower mass halos). In comparison, for  $d_{\text{iso}} = 50$  kpc, SMBHs are more numerous and at a given redshift tend to occupy lower mass halos.

In general, the most massive halos,  $> 10^{10} M_{\odot}$ , have the highest occupation fractions of SMBHs. By  $z = 10$  this

occupation fraction is close to unity for  $d_{\text{iso}} = 50$  kpc and slightly smaller for  $d_{\text{iso}} = 100$  kpc. However, the fraction of  $> 10^9 M_{\odot}$  halos at  $z = 10$  that host SMBHs is only  $0.16$  for  $d_{\text{iso}} = 50$  kpc and  $0.05$  for  $d_{\text{iso}} = 100$  kpc. These small fractions indicate the sparseness of SMBHs among these early galaxies for these relatively large values of  $d_{\text{iso}}$ . This suggests that in these models mergers of SMBHs will continue to be relatively rare at  $z < 10$ , especially for the  $d_{\text{iso}} = 100$  kpc case.

### 3.4 Synthetic Sky Maps

Given the considerations of the local SMBH number density and the results shown in Figure 1, we again focus on the

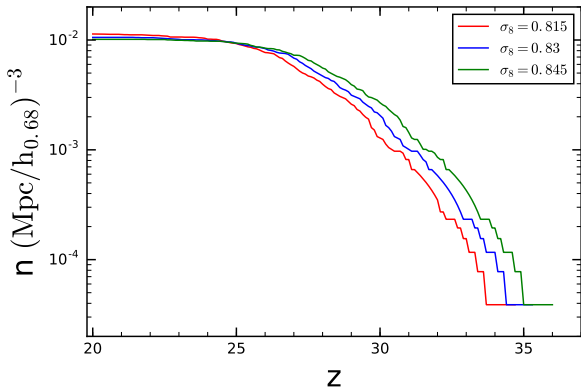


**Figure 6.** Effect of  $\sigma_8$  uncertainties on the evolution of comoving total number density of Pop III.1 stars and their SMBH remnants for  $d_{\text{iso}} = 100$  kpc, based on simulations of a  $(29.52 h_{0.68}^{-1} \text{Mpc})^3$  volume.

cases of  $d_{\text{iso}} = 50$  and 100 kpc, with the latter being the preferred, fiducial case. For reference, at  $z = 10, 15, 20, 30, 40$  the angular size of the box is  $21.53', 19.84', 18.93', 17.93', 17.37'$ , respectively.

To make an approximate synthetic sky map of the SMBH population (which may manifest themselves as AGN), we simply project through the entire volume of the box, adopting a constant, fixed redshift. This approximation ignores the finite light travel time across the thickness of the box, which means that the projection of the total source population is roughly equivalent to observing a finite redshift interval of the real universe. At  $z = 10, 15, 20$  these redshift intervals are  $\Delta z = 0.28, 0.49, 0.75$ , respectively. Of course for direct comparison with AGN populations one would also need to model the duty cycle of emission and the luminosity function and spectral energy distribution properties of the accreting SMBHs. Such modeling requires making many uncertain assumptions and is beyond the scope of the present paper, but will be addressed in future studies. More direct comparisons of the sky maps of the sources can in principle be done with other theoretical models and simulations that also aim to predict SMBH locations, along with the angular correlation function of the sources, discussed below.

Figure 8 shows maps of the Pop III.1 Star and SMBH remnant populations for  $d_{\text{iso}} = 50, 100, 300$  kpc at  $z = 10$ , for the three different values of  $t_{*f} = 10, 30, 100$  Myr. For smaller  $d_{\text{iso}}$  and longer  $t_{*f}$ , there are greater numbers of Pop III.1 stars present at  $z = 10$ .

This figure shows the dramatic effect of  $d_{\text{iso}}$  on the number of SMBH remnants predicted by the model, i.e., there is about a factor of 10 reduction in the number density of SMBHs on increasing  $d_{\text{iso}}$  from 50 kpc to 100 kpc. The angular clustering properties of these sources will be examined below.

Figure 9 shows synthetic maps at  $z = 10$  and 15, but now separating out different mass halos that are hosting Pop III.1 stars and SMBHs for the cases of  $d_{\text{iso}} = 50$  and 100 kpc (for  $t_{*f} = 10$  Myr). The evolution of the typical SMBH host halo towards higher masses as the universe evolves towards lower redshift can be seen. The lower mass halos tend to be the SMBHs that have formed most recently and, at least in

the  $d_{\text{iso}} = 50$  kpc case where there are significant numbers, these show distinctive clustering properties compared to the more massive, typically older, sources.

### 3.5 Angular Correlation

We calculate the two point angular correlation function (2PACF) of  $d_{\text{iso}} = 50$  and 100 kpc SMBH remnants. The angular correlation function tells us how the projection of these remnants is correlated compared to a Poisson distribution. We use a random catalog with 50 times the number of halos as in the SMBH sample, implementing the Landy-Szalay estimator to calculate the angular correlation function,  $\omega(\theta)$ :

$$\omega(\theta) = \frac{DD - 2DR + RR}{RR}, \quad (2)$$

where  $DD$  represents the total weight of pairs of halos from the data (i.e., the SMBHs) within each bin,  $RR$  represents the weight of pairs from the random Poisson catalog, and  $DR$  represents the weight of pairs with one particle from the data and one from the random catalog. We used the *TreeCorr* code (Jarvis et al. 2004) for these angular correlation calculations.

Figure 10 shows  $\omega(\theta)$  for the cases of  $d_{\text{iso}} = 50$  and 100 kpc observed at  $z = 10$  (i.e., derived from the spatial distributions shown in Fig. 8 for the case with  $t_{*f} = 10$  Myr). These have 27,122 and 1,913 SMBH sources, respectively. To increase the signal to noise we have observed the simulation volume at  $z = 10$  from the three orthogonal directions and combined the results. Overall the 2PACFs of both cases are relatively flat, especially compared to that of all halos with masses  $> 10^9 M_{\odot}$ , which is shown by the green dashed line in these figures. For  $d_{\text{iso}} = 50$  kpc, there is a sign of modest excess clustering signal on angular scales  $\lesssim 50''$ . For  $d_{\text{iso}} = 100$  kpc, with a smaller number of sources and thus larger Poisson uncertainties, there is hint of a decrease of  $\omega(\theta)$  below the Poisson level on scales  $\lesssim 50''$ . This could be related to the angular scale of the 100 kpc proper distance of the isolation (i.e., feedback) distance  $d_{\text{iso}}$  at  $z \sim 30$ , which corresponds to a comoving distance of  $\sim 3$  Mpc. By  $z = 10$  this corresponds to an angular scale of  $64''$ . Thus the signature of feedback cleared bubbles, which have a deficit of SMBHs due to destruction of Pop III.1 seeds, may be revealed in the angular correlation function. In particular, effective feedback suppression of neighboring sources leads to a relatively flat angular correlation function.

## 4 DISCUSSION AND CONCLUSIONS

We have presented a simple model for the formation of supermassive black holes from the remnants of special Population III stars, i.e., Pop III.1 stars that form in isolation from other astrophysical sources. The physical mechanism motivating this scenario involves the Pop III.1 protostar being supported by WIMP dark matter annihilation heating (Spolyar et al. 2008; Natarajan et al. 2009; Rindler-Daller et al. 2015), so that it retains a large photospheric radius while it is accreting. This reduces the influence of ionizing feedback on the protostar's own accretion (McKee & Tan 2008; Hosokawa et al. 2011), allowing it gather most of the

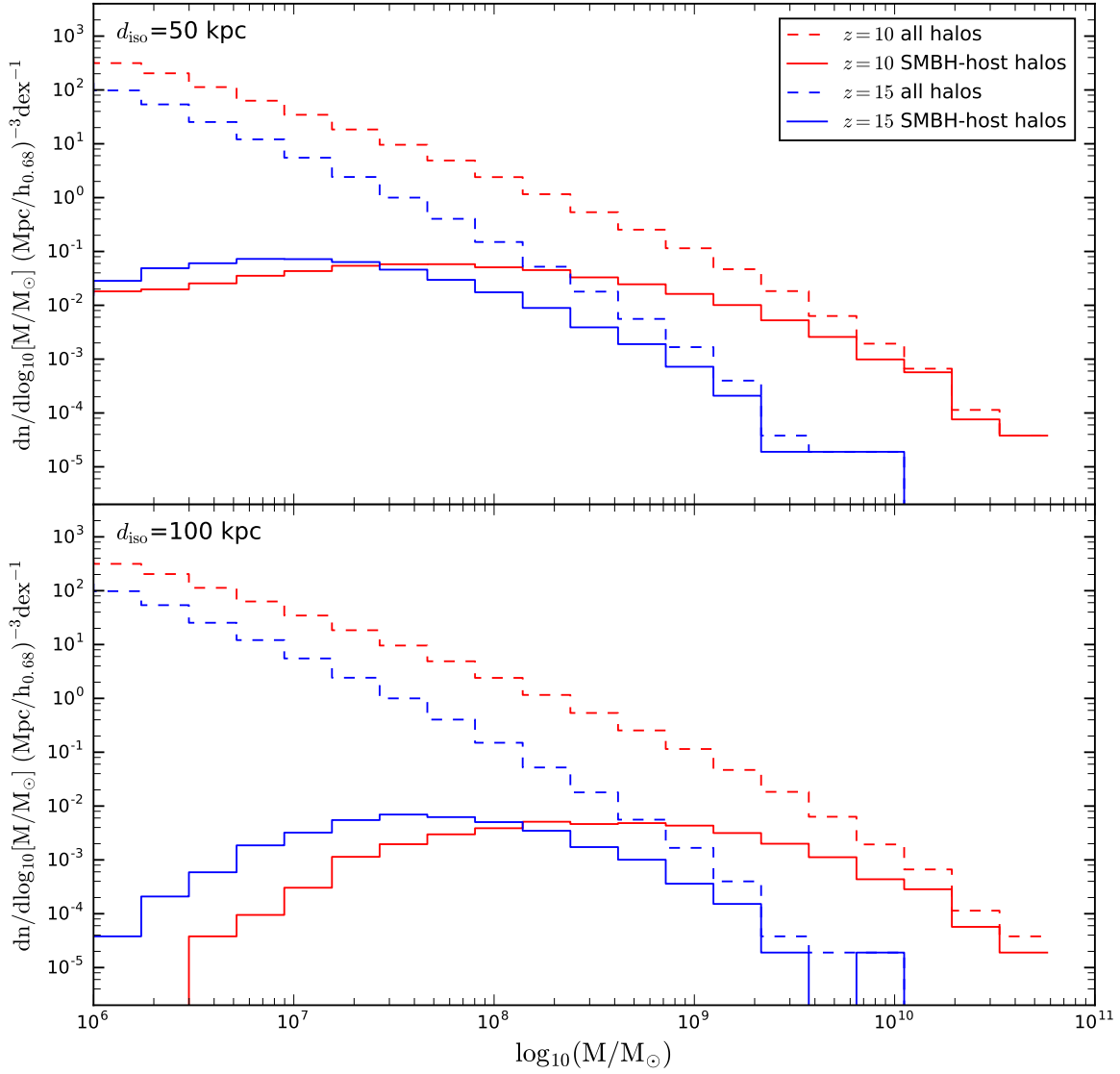


**Figure 7.** The mass functions of SMBH-host halos (solid lines) compared to all halos (dashed lines) at  $z = 10$  (red lines) and  $z = 15$  (blue lines). Results for  $d_{\text{iso}} = 50 \text{ kpc}$  are shown in the top panel, while those for  $d_{\text{iso}} = 100 \text{ kpc}$  are shown in the bottom panel. These results are based on the fiducial simulation of a  $(60.47 h_{0.68}^{-1} \text{ Mpc})^3$  volume.

$\sim 10^5 M_{\odot}$  of baryons present in the host minihalo. Such a mechanism may naturally explain the dearth of SMBHs with masses below  $\sim 10^5 M_{\odot}$ . While many of the details of this scenario remain to be explored, our approach here has been to focus on the Pop III.1 star and remnant SMBH populations that are predicted to form in such a model, particularly their dependencies on the isolation distance,  $d_{\text{iso}}$ , needed for Pop III.1 star formation.

Assuming that all SMBHs are produced by this mechanism, we have found that to produce the required number

density of sources that can explain local ( $z = 0$ ) SMBH populations requires  $d_{\text{iso}} \lesssim 100 \text{ kpc}$  (proper distance). For the model with  $d_{\text{iso}} = 100 \text{ kpc}$  and SMBH formation times  $t_{*f} = 10 \text{ Myr}$ , the formation of Pop III.1 stars and thus SMBHs starts to become significant at  $z = 35$ , peaks at  $z \simeq 30$  and is largely complete by  $z = 25$ , i.e., occurring in a period from only  $\sim 80 \text{ Myr}$  to  $\sim 130 \text{ Myr}$  after the Big Bang. This result can be understood with a simple physical model: the comoving number density of SMBHs is  $n_{\text{SMBH}} \sim (4\pi \tilde{d}_{\text{iso},z=30}^3/3)^{-1} \rightarrow 8.8 \times 10^{-3} (\tilde{d}_{\text{iso},z=30}/3 \text{ Mpc})^{-3} \text{ Mpc}^{-3}$ ,

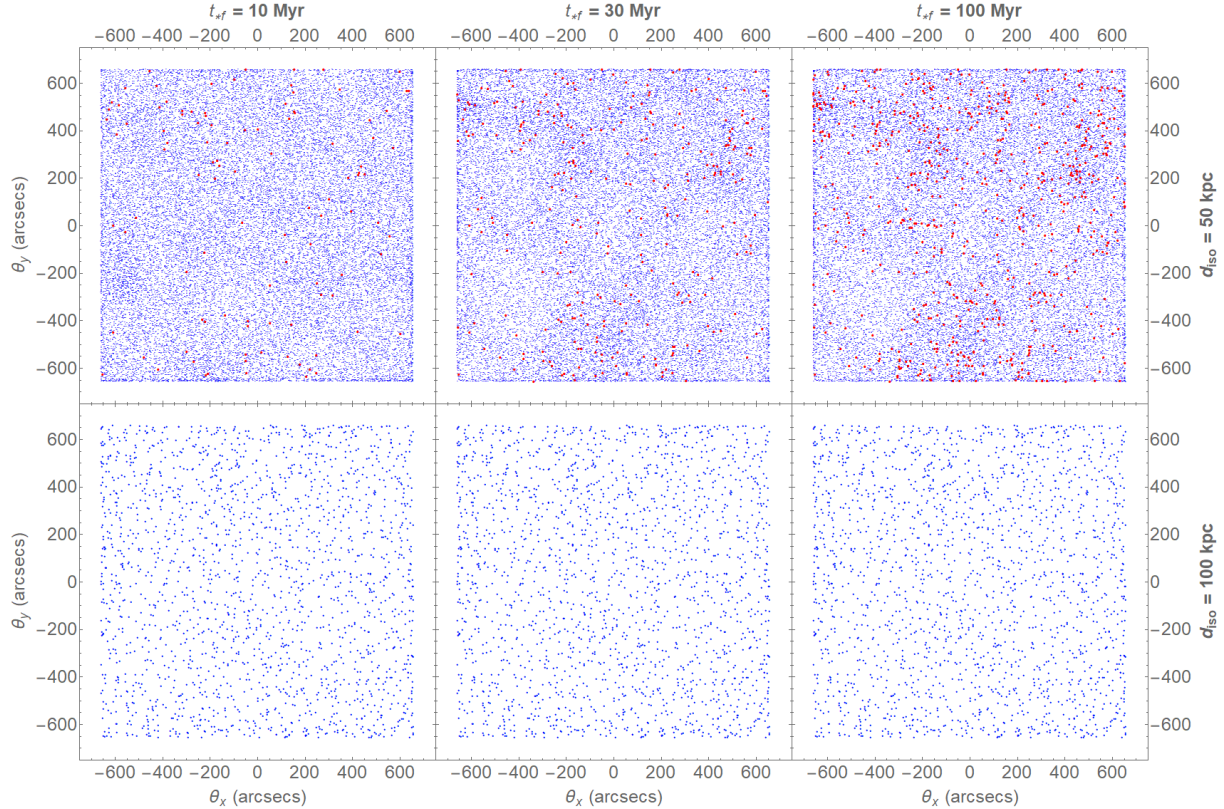


**Figure 8.** Synthetic sky maps at  $z = 10$  of the  $(60.47 h_{0.68}^{-1} \text{ Mpc})^3$  comoving box (projection equivalent to  $\Delta z = 0.28$ ) of the  $d_{\text{iso}} = 50$  kpc model (top row) with Pop III.1 stars (red dots) and SMBH remnants (blue dots). The panels from left to right show the cases with  $t_{*f} = 10, 30, 100$  Myr. The bottom row shows the same for  $d_{\text{iso}} = 100$  kpc (but note that in these cases there are no Pop III.1 stars left by  $z = 10$  even for  $t_{*f} = 100$  Myr).

where  $\tilde{d}_{\text{iso},z=30}$  is the comoving distance at  $z = 30$  corresponding to proper distance  $d_{\text{iso}}$ . Note, with such values of  $d_{\text{iso}}$  we do not expect SMBH mergers to be too significant in reducing their global comoving number density. Full predictions of merger rates evaluated down to  $z = 0$  will be presented in a future paper.

Compared to the “direct collapse” scenario of SMBH formation (e.g., Chon et al. 2016), the Pop III.1 protostar progenitor model we have presented involves much earlier and widespread formation of SMBHs. Thus there are expected to be significant differences in AGN luminosity functions at  $z \gtrsim 20$  between these models, i.e., there are much larger number densities of AGNs at these high redshifts in the Pop III.1 formation scenario.

We have followed the SMBH population to  $z = 10$ . By this redshift, SMBHs tend to reside in halos  $\gtrsim 10^8 M_{\odot}$ , extending up to  $\sim 10^{11} M_{\odot}$ . The angular correlation function of these sources at  $z = 10$  is very flat, with little deviation from a random distribution, which we expect is a result of a competition between source feedback and the intrinsic clustering expected from hierarchical structure formation.

The models presented here, being first approaches for describing the cosmic distribution of Pop III.1 sources, are intended to be simple and involve relatively few free parameters. Of course, much more detailed exploration of the growth and feedback of supermassive Pop III.1 stars and

their accreting SMBH remnants is still needed in the context of this scenario, both to explore the viability of forming SMBHs from Pop III.1 sources themselves and how their local feedback may limit other Pop III.1 star and SMBH formation, i.e., setting the value of  $d_{\text{iso}}$ . Diffuse feedback, e.g., from a Lyman-Werner FUV background due to widespread early stellar populations, i.e., Pop III.2 and Pop II stars, may also need to be considered depending on the formation efficiencies and IMFs of these populations. Such a diffuse background feedback could act to effectively truncate new Pop III.1 star formation below a certain redshift, independent of local feedback that we have so far parameterized via  $d_{\text{iso}}$ .

We defer exploration of these types of models, which have additional free parameters, to future studies. Other future work will include tests of the models that involve modeling the potentially observable luminosity functions of Pop III.1 and SMBH sources at high redshift and following the populations of SMBHs down to  $z = 0$  to compare with the observed clustering properties of the local SMBH population.

**Acknowledgments** – We thank Peter Behroozi, Kritapas Chanchaiworawit, Mark Dijkstra, Alister Graham, Lucio Mayer, Rowan Smith, Kei Tanaka, Brian Yanny and an anonymous referee for helpful comments and discussions. Fermilab is operated by Fermi Research Alliance, LLC, un-

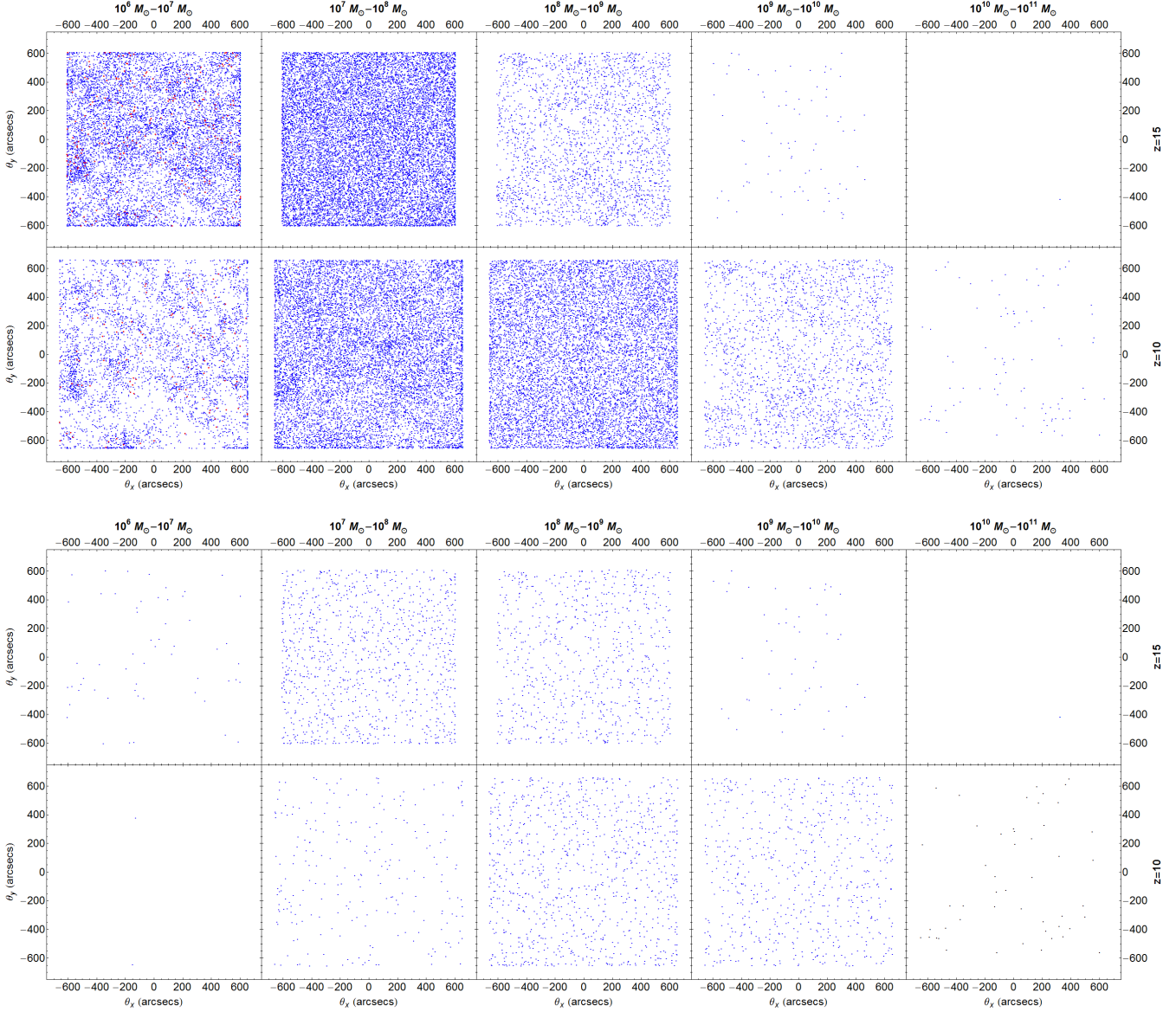


**Figure 9.** (a) *Top panel:* Synthetic maps at  $z = 15$  (top row) and  $z = 10$  (bottom row) of  $d_{\text{iso}} = 50$  kpc Pop III.1 stars (assuming  $t_{*f} = 10$  Myr) (red dots) and SMBH remnants (blue dots) for mass bins from left column to right column of  $10^6 - 10^7 M_{\odot}$ ,  $10^7 - 10^8 M_{\odot}$ ,  $10^8 - 10^9 M_{\odot}$ ,  $10^9 - 10^{10} M_{\odot}$  and  $10^{10} - 10^{11} M_{\odot}$ . (b) *Bottom panel:* As (a), but now for  $d_{\text{iso}} = 100$  kpc. Pop III.1 stars are present at  $z = 10$  and  $z = 15$  only for  $d_{\text{iso}} = 50$  kpc and they have mass in the range  $10^6 - 10^7 M_{\odot}$ .

der Contract No. DE-AC02-07CH11359 with the U.S. Department of Energy. NB acknowledges the support by the Fermilab Graduate Student Research Program in Theoretical Physics. NB also acknowledges the support of the D-ITP consortium, a programme of the Netherlands Organization for Scientific Research (NWO) that is funded by the Dutch Ministry of Education, Culture and Science (OCW). JCT acknowledges support from NSF grant AST 1212089 and ERC Advanced Grant 78882 (MSTAR).

## REFERENCES

- Abel, T, Bryan, G. L., & Norman M. L. 2002, *Science*, 295, 93
- Ackermann, M. et al. (Fermi-LAT Collaboration) 2015, *Phys. Rev. Lett.* 115, 221301
- Agnese, R. et al. (SuperCDMS Collaboration) 2014, *Phys. Rev. Lett.* 112, 241302.
- Aguirre, J. E., Ginsburg, A. G., Dunham, M. K., et al. 2011, *ApJS*, 192, 4
- Ahn, C. P., Seth, A. C., Den Brok, M. et al. 2017, *ApJ*, accepted (arXiv:1703.09221)
- Akerib, D. S. et al. 2016, *Phys. Rev. Lett.* 116, 161302.
- Akerib, D. S. et al. 2017, *Phys. Rev. Lett.* 118, 251302.
- Amole, C. et al. 2017, *Phys. Rev. Lett.* 118, 251301.
- Baldassare, V. F., Reines, A. E., Gallo, E., & Greene, J. E. 2015, *ApJ*, 809, L14
- Barber C., Schaye J., Bower R. G., Crain R. A., Schaller M., Theuns T., 2016, *MNRAS*, 460, 1147

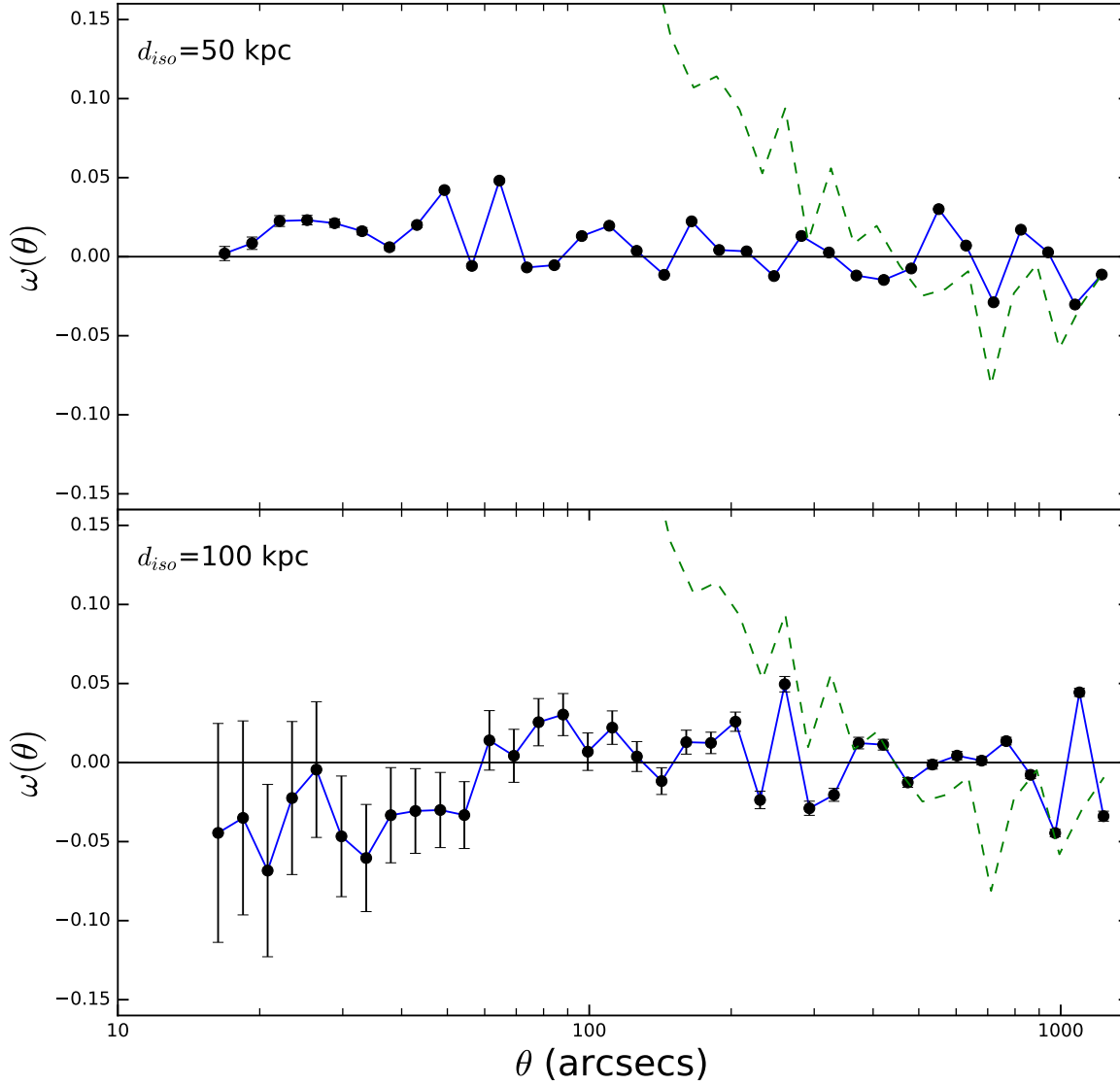


**Figure 10.** 2PCF (black points and blue solid line) of  $d_{\text{iso}} = 50\text{kpc}$  (top panel) and  $d_{\text{iso}} = 100\text{kpc}$  (bottom panel) remnants at  $z = 10$ . The error bars indicate shot noise in each angular separation bin. For comparison we have also plotted the 2PCF of all the halos with masses  $> 10^9 M_{\odot}$  at  $z = 10$  (green dashed lines). It rises sharply at small scales, which shows they are highly clustered (it reaches a value of 0.22 at  $100''$  and 0.57 at  $20''$ ). The SMBHs in these models show much lower levels of clustering on small angular scales due to feedback suppression of neighboring halos that prevents them from being Pop III.1 sources.

Baumgardt, H. 2017, MNRAS, 464, 2174  
 Baumgarte, T. W., & Shapiro, S. L. 1999, ApJ, 526, 941  
 Begelman, M. C., Volonteri, M., & Rees, M. J. 2006, MNRAS, 370, 289  
 den Brok, M., Seth, A. C., Barth, A. J. et al. 2015, ApJ, 809, 101  
 Bromm, V. 2013, Rep. Prog. Phys., 76, 11  
 Bromm, V., Coppi, P. S. & Larson, R. B. 2002, ApJ, 564, 23

Bromm, V. & Loeb, A. 2003, ApJ, 596, 34  
 Buchert, T. & Ehlers, J. 1993, MNRAS, 264, 375  
 Catelan, P. 1995, MNRAS, 276, 115  
 Chandrasekhar, S. 1964, ApJ, 140, 417  
 Chon, S., Hirano, S., Hosokawa, T., & Yoshida, N. 2016, ApJ, 832, 134  
 Clark, P. C., Glover, S. C. O., Smith, R. J., Greif, T. H., Klessen, R. S., & Bromm, V. 2011, Science, 331, 1040  
 Cowie, L. L., Barger, A. J. & Hasinger, G. 2012, ApJ, 748,



- 50
- Devecchi, B., Volonteri, M., Rossi, E. M., Colpi, M., & Portegies Zwart, S. 2012, *MNRAS*, 421, 1465
- Di Matteo, T., Colberg, J., Springel, V., Hernquist, L., Sijacki, D. 2008, *ApJ*, 676, 33
- Dijkstra, M., Haiman, Z., & Spaans, M. 2006, *ApJ*, 649, 14
- Dijkstra, M., Ferrara, A., & Mesinger, A. 2014, *MNRAS*, 442, 2036
- Farrell, S. A., Servillat, M., Gladstone, J. C. et al. 2014, *MNRAS*, 437, 1208
- Feng H., Rao F. & Kaaret P. 2010, *ApJ*, 710, L137
- Feng H. & Soria R. 2011, *New Astronomy Reviews*, 55, 166
- Ferrara, A. & Loeb, A. 2013, *MNRAS*, 431, 2826
- Fialkov, A., Barkana, R., Tseliakhovich, D., & Hirata, C. M. 2012, *MNRAS*, 424, 1335
- Fiore, F., Puccetti, S., Grazian, A. et al. 2012, *A&A*, 537, 16
- Fontanot, F., Monaco, P. & Shankar, F. 2015, *MNRAS*, 453, 4112
- Freese, K., Ilie, C., Spolyar, D. et al. 2010, *ApJ*, 716, 1397
- Freitag, M., Gürkan, M. A., & Rasio, F. A. 2006, *MNRAS*, 368, 141
- Graham, A. W. 2016, *ASSL*, 418, 263
- Graham, A. W., Scott, N. 2015 *ApJ*, 798, 54
- Graham, A. W., Onken, C. A., Athanassoula, E., & Combes, F. 2011, *MNRAS*, 412, 2211
- Greif, T. H. & Bromm, V. 2006, *MNRAS*, 373, 128
- Greif, T. H., Springel, V., White, S. D. M., Glover, S. C. O., Clark, P. C., Smith, R. J., Klessen, R. S. & Bromm, V. 2011a, *ApJ*, 737, 75
- Greif, T. H., White, S. D. M., Klessen, R. S. & Springel, V. 2011b, *ApJ*, 737, 75
- Gürkan, M. A., Freitag, M., & Rasio, F. A. 2004, *ApJ*, 604, 632
- Haehnelt, M. G. & Rees, M. J. 1993, *MNRAS*, 263, 168
- Hennebelle, P., Commerçon, B., Joos, M. et al. 2011, *A&A*, 528, 72
- Hirano, S., Hosokawa, T., Yoshida, N. et al. 2014, *ApJ*, 781, 60
- Hirano, S., Hosokawa, T., Yoshida, N. & Kuiper, R. 2017, *Science*, 357, 1375
- Hosokawa, T., Omukai, K., Yoshida, N. & Yorke, H. W. 2011, *Science*, 334, 1250
- Hosokawa, T., Hirano, S., Kuiper, R., Yorke, H. W., Omukai, K., & Yoshida, N. 2016, *ApJ*, 824, 119
- Inayoshi, K. & Omukai, K. 2012, *MNRAS*, 422, 2539
- Inayoshi, K., Hosokawa, T. & Omukai, K. 2013, *MNRAS*, 431, 3036
- Inayoshi, K., Visbal, E., & Kashiyama, K. 2015, *MNRAS*, 453, 1692
- Jarvis, M., Bernstein, G., & Jain, B. 2004, *MNRAS*, 352, 338
- Johnson, J. L., & Bromm, V., 2007, *MNRAS*, 374, 1557
- Khachatryan, V. et al. (CMS Collaboration) 2016, *Phys. Rev. D*, 93, 052011
- Kirsten, F. & Vlemmings, W. H. T. 2012, *A&A*, 542, 44
- Kızıltan, B., Baumbardt, H. & Loeb, A. 2017, *Nature*, 542, 203
- Kormendy, J. & Ho, L. C. 2013, *ARA&A*, 51, 511
- Latif, M. A. & Schleicher, D. R. G. 2016, *A&A*, 585, 151
- Mayer, L., Kazantzidis, S., Escala, A., & Callegari, S. 2010, *Nature*, 466, 1082
- Mayer, L., Fiacconi, D., Bonoli, S., Quinn, T., Roskar, R., Shen, S. & Wadsley, J. 2015, *ApJ*, 810, 51
- McKee, C. F. & Tan, J. C. 2008, *ApJ*, 681, 771
- Milosavljević, M., Bromm, V., Couch, S. M., & Oh, S. P. 2009, *ApJ*, 698, 766
- Monaco, P. 2016, *Galaxies*, vol. 4, issue 4, p. 53
- Monaco, P., Theuns, T., & Taffoni, G. 2002, *MNRAS*, 331, 587
- Monaco, P., Sefusatti, E., Borgani, S. et al. 2013, *MNRAS*, 433, 2389
- Mortlock, D. J., Warren, S. J., Venemans, B. P. et al. 2011, *Nature*, 474, 616
- Moutarde, F., Alimi, J.-M., Bouchet, F. R. et al. 1991, *ApJ*, 382, 377
- Munari, E., Monaco, P., Sefusatti, E. et al. 2016, *arXiv:1605.04788*
- Natarajan, A., Tan, J. C. & O'Shea, B. W. 2009, *ApJ*, 692, 574
- Norberg, P., Cole, S., Baugh, C. et al. 2002, *MNRAS*, 336, 907
- O'Shea, B. W., Abel, T., Whalen, D. & Norman, M. L. 2005, *ApJ Lett.*, 628, L5
- O'Shea, B. W. & Norman, M. L. 2006, *ApJ*, 654, 66
- Pasham D. R., Strohmayer T. E. & Mushotzky R. F. 2014, *Nature*, 513, 74
- Pintore, F., Zampieri, L., Sutton, A. D. et al. 2016, *MNRAS*, 459, 455
- Planck Collaboration: Ade, P. A. R., Aghanim, N., Arnaud, M. et al. 2015, *arXiv:1502.01589*
- Planck Collaboration: Adam, R., Aghanim, N., Ashdown, M. et al. 2016, *A&A*, 596, 108
- Portegies Zwart, S. F., Baumgardt, H., Hut, P., Makino, J., & McMillan, S. L. W. 2004, *Nature*, 428, 724
- Price, D. J. & Bate, M. R. 2007, *MNRAS*, 377, 77
- Reed, D. S., Bower, R., Frenk, C. S., Jenkins, A., Theuns, T. 2007, *MNRAS*, 374, 2
- Rees, M. J. 1978, *The Observatory*, 98, 210
- Reines, A. E. & Comastri, A. 2016, *PASA*, 33, 54
- Rindler-Daller, T., Montgomery, M. H., Freese, K., Winget, D. E. & Paxton, B. 2015, *ApJ*, 799, 210
- Schauer, A. T. P., Regan, J., Glover, S. C. O., Klessen, R. S. 2017, *MNRAS*, 471, 4878
- Schleicher, D. R. G., Banerjee, R., Sur, S. et al. 2010, *A&A*, 522, 115
- Schober, J., Schleicher, D. R. G., Federrath, C. et al. 2012, *ApJ*, 754, 99
- Seth, A. C., van den Bosch, R., Mieske, S., et al. 2014, *Nature*, 513, 398
- Shankar, F., Bernardi, M., Sheth R. K. et al. 2016, *MNRAS*, 460, 3119
- Shapiro, P. R., Iliev, I. T., & Raga, A. C. 2004, *MNRAS*, 348, 753
- Shirakata, H., Kawaguchi, T., Okamoto, T. et al. 2016, *MNRAS*, 461, 4389
- Sijacki, D., Springel, V., Di Matteo, T., & Hernquist, L. 2007, *MNRAS*, 380, 877
- Smith, R. J., Iocco, F., Glover, S. et al. 2012, *ApJ*, 761, 154
- Somerville, R. S., Hopkins, P. F., Cox, T. J., Robertson, B. E., Hernquist, L. 2008, *MNRAS*, 391, 481
- Spolyar, D., Bodenheimer, P., Freese, K., & Gondolo, P. 2009, *ApJ*, 705, 1031

- Spolyar, D., Freese, K., & Gondolo, P. 2008, *Phys. Rev. Lett.*, 100, 051101
- Stacy, A., Pawlik, A. H., Bromm, V. & Loeb, A. 2014, *MNRAS*, 441, 822
- Susa, H., Hasegawa, K. & Tominaga, N. 2014, *ApJ*, 792, 32
- Tselikhovich, D., & Hirata, C. 2010, *Phys. Rev. D*, 82, 083520
- Tan, J. C. & Blackman, E. G. 2004, *ApJ*, 603, 401
- Tan, J. C. & McKee, C. F. 2004, *ApJ*, 603, 383
- Tan, J. C., Smith B. D., & O'Shea, B. W. 2010, *AIPC*, 1294, 34
- Tanaka, K. E. I., Tan, J. C. & Zhang, Y. 2017, *ApJ*, in press (arXiv:1610.08856)
- Tanaka, T. L. & Li, M. 2014, *MNRAS*, 439, 1092
- Treister, E., Schawinski, K., Volonteri, M. & Natarajan, P. 2013, *ApJ*, 778, 130
- Turk, M. J., Abel, T. & O'Shea, B. W. 2009, *Science*, 325, 601
- Umeda, H., Hosokawa, T., Omukai, K. & Yoshida, N. 2016, *ApJ*, 830, L34
- Vink, J. S. 2008, *New Astron. Rev.*, 52, 419
- Vika, M., Driver, S. P., Graham, A. W. and Liske, J. 2009, *MNRAS*, 400, 1451.
- Vito, F., Gilli, R., Vignali, C. et al. 2016, *MNRAS*, 463, 348
- Vogelsberger, M., Genel, S., Springel, V. et al. 2014, *Nature*, 509, 177
- Watson, W. A., Iliiev, I. T., Diego, J. M. et al. 2014, *MNRAS*, 437, 3776
- Whalen, D. & Norman, M. L. 2006, *ApJS*, 162, 281
- Whalen, D., O'Shea, B. W., Smidt, J., & Norman, M. L. 2008, *ApJ*, 679, 925
- Willott, C. J., Delorme, P., Reyl e, C. et al. 2010, *AJ*, 139, 906
- Wrobel, J. M., Miller-Jones, J. C. A. & Middleton, M. J. 2016, *AJ*, 152, 22
- Zampieri L. & Roberts T. P. 2009, *MNRAS*, 400, 677
- Zocchi, A., Gieles, M. & H enault-Brunet, V. 2016, *IAUS*, 312, 197